




Anisotropization of quasistatic magnetohydrodynamic turbulence with an increasing magnetic field: Transition from three to two dimensions

Semion Sukoriansky ^{1,*},† Eli Barami ^{1,2,*},‡ Yuri Feldman ¹ and Efi Zemach^{1,2,3}

¹*Department of Mechanical Engineering, Ben-Gurion University of the Negev, Beer-Sheva, Israel*

²*SOREQ Nuclear Research Center, Israel*

³*Department of Mechanical Engineering, Sami Shamoon College of Engineering, Beer-Sheva, Israel*



(Received 26 September 2021; accepted 28 June 2022; published 25 July 2022)

We studied the anisotropization of homogeneous magnetohydrodynamic turbulence at low magnetic Reynolds numbers. Flows of this type are not only important for different engineering applications, but also provide an appealing framework for studies of quasi-two-dimensional turbulence with strongly modified transport properties. The results of large-scale forced, direct numerical simulations are presented and compared with those obtained with the quasi-normal scale elimination theory. For a weak magnetic field, the simulations validated the theoretical predictions, including the generation of the $k^{-7/3}$ range of the energy spectra and its propagation toward higher wave numbers with increasing magnetic field strength. In a strong magnetic field, the turbulence attains a quasi-two-dimensional state with an enstrophy cascade inertial range of the normal flow components in the normal plane and a passive scalar inertial-convective range of the parallel component. The corresponding energy spectra are in a good agreement with logarithmically corrected k^{-3} and k^{-1} theoretical predictions. With increasing Reynolds number at constant magnetic field the enstrophy cascade becomes unstable and is replaced by helicity cascade with $k^{-7/3}$ energy spectrum. The enstrophy cascade is restored with an increasing magnetic field. An investigation of the mechanism of energy injection into the parallel component in a strong magnetic field revealed that the energy is supplied directly by an external force. The spectrum of the parallel component depends on the isotropy of external forcing and is, thus, not universal.

DOI: [10.1103/PhysRevFluids.7.074607](https://doi.org/10.1103/PhysRevFluids.7.074607)

I. INTRODUCTION

Turbulent flows in the atmosphere, in the oceans, and in engineering devices are often affected by external body forces, which render them anisotropic. Buoyancy, the Coriolis force, and the Earth's curvature are the main factors leading to anisotropization of large-scale atmospheric and oceanic flows and subsequent significant modification of turbulence dynamics. Another important example of anisotropic turbulence is the turbulent flow of an electrically conducting fluid placed in a permanent external magnetic field. In particular, magnetohydrodynamic (MHD) flows of liquid metals are important for many engineering applications, including liquid-metal heat exchangers, MHD pumps, and metallurgy applications [1,2]. A characteristic feature of liquid metals is their low magnetic Prandtl number, $Pr_m = \nu_0/\kappa \ll 1$ (where ν_0 and κ are the kinematic viscosity and magnetic diffusivity, respectively). Thus, liquid-metal flows are typically fully turbulent with large

*These authors contributed equally to this work.

†semion@bgu.ac.il

‡elli@post.bgu.ac.il

hydrodynamic Reynolds numbers, Re , and small magnetic Reynolds numbers, Re_m . When Re_m is small, the Lorentz force can be reduced to the anisotropic ohmic (Joule) dissipation term in the Navier-Stokes equation [3,4], and the ensuing approximation is known as “quasistatic (QS)-MHD.” The dissipation term causes a suppression of velocity fluctuations along the direction of the magnetic field.

In the past few decades, a great deal of effort has been invested in studying the effect of a permanent magnetic field on QS-MHD turbulence. It has been found experimentally that if the field is sufficiently strong, the wall friction and the drop in the channel flow pressure approach the laminar limit, while the velocity fluctuations in the direction normal to the field remain strong [5–8]. These phenomena—together with the experimentally observed increase of the velocity correlation length in the direction of the field [9], the suppression of vortices with axes perpendicular to the field, and the stabilization of vortices with axes parallel to the field [10–13]—indicate the tendency of liquid-metal turbulence to attain a quasi-two-dimensional (2D) state under the action of a permanent magnetic field [5,6,14–16]. Liquid-metal MHD flows (which can be replicated under controllable laboratory experiments) provide a convenient framework for studies of quasi-2D turbulence with anisotropic transport properties [16–18] and of the mechanism of transition from an isotropic three-dimensional (3D) state to a quasi-2D state. The peculiar features of anisotropic turbulence, such as an inverse energy cascade typical of forced 2D turbulence [19], have been observed experimentally [20].

Complete two dimensionality, even at high magnetic field, cannot be achieved in the presence of solid boundaries where Hartmann boundary layers, developed along walls perpendicular to the field, preclude its formation. Klein *et al.* [21] studied a vortex pair created by injecting electric current into a thin layer of liquid metal under an externally imposed, transverse magnetic field. They found that columnar vortices have different rotation rates on top and bottom walls, and wobble when the injected current is high enough. Klein and Potherat [22] generated quasi-2D flow in a cubic container by injecting an array of electric currents locally at one wall. They also found that the quasi-2D vortices are less intense near the top wall. This indicates that each columnar vortex undergoes differential rotation termed by the authors “weak form of three-dimensionality.” Strong three dimensionality is characterized by vortex disruption and is scale selective: For narrow vortices with large aspect ratios, the time of Joule diffusion (diffusion of momentum by the Lorentz force) exceeds the vortex turnover time, inertial effects disrupt them, so they become 3D. A cutoff scale separates vortices that are “wide” enough to be quasi-2D from the smaller 3D vortices. These results were further elaborated in a more detailed experiment on the same experimental facility [23]. It was found that, unlike for domains with nondissipative boundaries, the transition between quasi-2D and 3D turbulence does not result from the global instability of the flow, but is rather a process that is controlled by the large-scale interaction parameter N . Both types of three dimensionality vanish only in the limit $N \rightarrow \infty$. Potherat and Klein [24] measured the intensity of turbulence with increasing magnetic field while keeping the force constant. Velocity gradients along the field are smoothed out by Joule diffusion as the field increases, causing reduction of Joule dissipation such that turbulent fluctuations retain more energy. The net effect is an increase of turbulent intensity.

The lack of transparency of liquid metals precludes the use of laboratory measurements for obtaining a complete description of the turbulent field in these media. Direct numerical simulation (DNS) is therefore applied to close the knowledge gap. Major experimental findings have been replicated and confirmed by DNS, among them the tendency of QS-MHD turbulence to attain a quasi-2D state in sufficiently strong magnetic fields [25–29]. Moreover, DNS can provide comprehensive description of the turbulent field and its modification under the impact of a magnetic field. For example, the simulations by Zikanov *et al.* [30] replicated all the complicated conditions of the laboratory experiment of Sukoriansky *et al.* [16], thereby throwing light on the mechanisms leading to the anomalous high-amplitude velocity fluctuations detected in the experiment. The simulation results were in good qualitative agreement with the experimental data, and the computed spatial structure and statistical properties of the flow did indeed provide an explanation for the experimental observations.

Although MHD flows at low Re_m have been studied extensively, most numerical studies to date were limited to high interaction parameters and turbulence two dimensionalization. Several investigations did, however, consider the range of weak to moderate magnetic fields, and three of these studies are reviewed in brief. Zikanov and Thess [25] studied the effect of a permanent magnetic field over a wide range of interaction parameters at relatively low resolution (up to 128^3 grid points). Steady state was achieved by keeping the energy of Fourier modes with $k < 2.5$ at a constant level. At high interaction parameters, $N_0 \gg 1$, the kinetic energy spectrum approached k^{-3} scaling typical of 2D turbulence. At an intermediate interaction parameter, $N_0 = 0.4$, computed with a lower resolution of 64^3 grid points, the system exhibited intermittent behavior, characterized by long periods of quasi-2D dynamics, interrupted by erratic bursts of 3D turbulence. This strongly intermittent behavior was not fully understood, but it was thought that the low computational resolution or the specific way of maintaining a statistically steady state might have played a considerable role. Thus, according to Zikanov and Thess [25], the turbulence behavior at moderate interaction parameters was well worth further detailed investigation. Note that the intermittency was only observed in simulations with periodic or nonslip boundary conditions. It was never observed in flows with dissipation at the boundaries. Reddy [31] performed DNS in a periodic box with a resolution of up to 512^3 grid points. His simulations performed with 256^3 grid points showed steepening of the energy spectrum as the interaction parameter increased. For $N_0 = 1.7$ and $N_0 = 5.5$, power laws of -3.2 and -3.8 , respectively, were observed. These simulations indicated that—unlike in 2D turbulence—vertical structures developed. The field became two dimensional at larger values of the interaction parameters, $11 \leq N_0 \leq 18$, with most of the energy being concentrated in the horizontal (perpendicular to the magnetic field) components of the velocity. With a further increasing field, the spectral power continued to decrease, and for a very large interaction parameter, $N_0 = 130$, exponential behavior was observed. Reddy [31] reported that at such a magnetic field the magnitudes of the horizontal and vertical flow components were comparable, and the flow behaved as 2D three-componential (2D-3C) turbulence. Burattini *et al.* [29] studied the anisotropy induced by a magnetic field. They performed DNS in a periodic box with a low resolution of 256^3 grid points and examined the traditional 3D and the longitudinal one-dimensional (1D) energy spectra. The 3D spectrum of the velocity component parallel to the field was found to be more energetic than that of the perpendicular component, similarly to the findings reported in Refs. [26,28], while the longitudinal 1D spectrum of the parallel component was attenuated at all scales. This result strongly depends on boundary conditions, as energy in the third component vanishes in turbulence bounded by Hartmann walls [32].

Potherat and Albuossiere [33], Dymkou and Potherat [34], and Potherat and Dymkou [35] developed a new spectral method for the direct numerical simulation of QS-MHD turbulence. The method relies on the basis of eigenmodes of the total dissipation operator, which includes viscous and Joule dissipation. The new basis is a subset of the Fourier space ordered by the increasing linear decay rate. It was shown [33] that the sequence of eigenfunctions can closely mimic the anisotropic properties of QS-MHD turbulence. By computing the set of least dissipative modes in the discrete space of Fourier coefficients, the authors found the upper bound for the attractor dimension. They concluded that expansions of solutions of the Navier-Stokes equations over the base of minimal eigenmodes might be suitable to calculate turbulent flows. This approach reduces the cost of DNS by confining the spectral domain of resolution to that relevant to the flow dynamics. In the case of the domain bounded by walls orthogonal to the magnetic field, the spectral analysis of the dissipation operator leads to a sequence of eigenfunctions that exhibit the correct Hartmann boundary layer profile in the vicinity of these walls [36].

Notwithstanding extensive experimental and numerical studies, fundamental questions related to the anisotropization of QS-MHD turbulence remain: How does an external uniform magnetic field modify the transport properties of MHD turbulence with small Re_m ? How does the anisotropization of different turbulent scales develop? What are the criteria for transition to quasi-2D dynamics? Analytical theories supported and complemented by DNS are needed to answer these questions. This is precisely the purpose of this paper, i.e., verification of the analytical predictions obtained

using the quasi-normal scale elimination (QNSE) theory [37] with those of high-resolution DNS, extension of the DNS into the high interaction parameter region not covered by the theory, and computation of turbulence parameters not derived from the QNSE theory. The QNSE results as applied to QS-MHD will be briefly explained in the next section. Immediately below we present a brief account of analytical results obtained using other theories.

A relatively simple approach to studying the development of anisotropy is to consider initially isotropic turbulence suddenly subjected to a uniform magnetic field and to neglect the viscous and nonlinear terms in the flow equations. This theory, known as the rapid distortion theory (RDT) [38–40], gives a qualitative picture of the initial stage of the turbulence reorganization. The Fourier modes located close to the axis parallel to the magnetic field (the so-called Joule cone) are damped most rapidly, and thus this part of the cone becomes depleted of energy first. As time progresses, energy removal affects modes at increasing angles, leading to an energy flux in the angular direction from the region outside the cone towards the cone axis [41,42]. A linear mechanism controls the evolution of turbulence over short times. Schumann [43] compared the full nonlinear simulations with otherwise identical linear simulations and found that the linear results agree with the nonlinear ones within 3% for only one-fifth of the large-scale turnover time. For longer times, nonlinearity has a cumulative effect that modifies the evolution of turbulence beyond a linear response.

The drawback of the RDT is that it has only limited predictive skills. More accurate theories describe nonlinear interactions explicitly, using a spectral approach and certain closure hypotheses. One of these closures, the eddy-damped quasi-normal Markovian (EDQNM) theory [44], has been applied to MHD turbulence [38,45,46]. The basic closure assumption of this theory is that the fourth-order spectral moments appearing in the equations for the third-order moments can be approximated as if the velocity fluctuations were Gaussian. The theory predicts transition from 3D turbulent flow to a “two-and-a-half-dimensional” flow [47] as a result of the combined effects of a short-term linear Joule dissipation and a longer-term nonlinear creation of polarization anisotropy. The transition is characterized by the elongation of turbulent structures along the applied magnetic field and by strong anisotropization of the directional two-point correlation spectra. Evolution of the initially isotropic homogeneous turbulence under the impact of an external magnetic field was studied in Ref. [46] in terms of directional and polarization anisotropy using the anisotropic EDQNM model. The authors used a Helmholtz-like poloidal-toroidal decomposition to derive all the algebra in terms of only the incompressible components. The poloidal-toroidal decomposition of the velocity field employed in Ref. [46], and the computation of a polarization tensor, made it possible to conclude whether the anisotropic mechanism is of a linear nature or is due to more complex nonlinear interactions. The most advanced model (EDQNM2) accounts for the anisotropic Joule dissipation in the equations for both the second- and the third-order moments. The results of EDQNM2 were compared with those of the simpler EDQNM1 model, which retains the Joule dissipation term only in the equation for the second-order moment. The comparison clarified the role of a nonlinear mechanism in turbulence anisotropization and proved that including the explicit effect of anisotropic Joule dissipation in the nonlinear dynamics is crucial for computation of strong anisotropy leading to ultimate two dimensionalization.

The linear and nonlinear mechanisms were further investigated in Ref. [46] using DNS of freely decaying QSMHD turbulence. The two-point second-order spectral tensor and related k - and angle-dependent toroidal and poloidal energy tensors were computed and compared with data derived from EDQNM models. The simulations revealed scale-dependent structure of the flow with dominance of transverse kinetic energy at large scales and a dominance of axial (along the direction of the magnetic field) kinetic energy at small scales. Departure from initial poloidal-toroidal equipartition of energy was most evident for the transverse wave vectors, where the energy accumulates because of ohmic dissipation. The description of very strong anisotropy, by means of angle-dependent spectra for directional energy and polarization, is the most important result of this study. The distribution of transverse and axial energy and enstrophy in the $(k_{\perp}, k_{\parallel})$ spectral space, the ratios of transverse to axial energy (enstrophy), and the off-diagonal components of the Reynolds stress tensor indicate that the flow dynamics approach 2D-3C state. Slopes k_{\perp}^{-3} and k_{\perp}^{-1} , typical of 2D-3C

flows, were observed, with the axial component acting as a passive scalar. The energy-transfer spectra were computed both in DNS and the EDQNM model and were used to describe in detail the most important dynamics of the ultimate anisotropic state.

The QNSE theory complements the EDQNM approach, as it allows for the calculation of eddy viscosities and eddy diffusivities, while the EDQNM computations yield energy transfers. The QNSE methodology has been applied to various turbulent flows, such as isotropic homogeneous turbulence with no extra strains [48], and to stably stratified [49], rotating [50], and QS-MHD flows [37]. Some of the most relevant cornerstones of the QNSE theory as applied to MHD turbulence with low Re_m are given in the Appendix.

The QNSE theory offers a novel description of QS-MHD turbulence, and although it was developed for weak magnetic fields, it can be extended to moderate fields beyond its small interaction parameter limit. The theory provides analytical expressions for the scale-dependent eddy viscosities and eddy diffusivities in the directions parallel and normal to the external magnetic field. Other turbulence properties, such as 1D and 3D energy spectra, are also analytically derived, thereby shedding light on the modification of the Kolmogorov $k^{-5/3}$ spectrum by anisotropic Joule dissipation. In particular, it is shown that a weak magnetic field generates $k^{-7/3}$ corrections to all 1D spectra. One of the goals of the present work is to examine the QNSE theory and to determine at which magnetic fields it is still valid by comparing the energy spectra predicted by the QNSE theory to those obtained by DNS.

DNS with up to 1024^3 grid points was employed to study the transition from isotropic to anisotropic turbulence at weak, moderate, and strong magnetic fields. The goal is to study properties at scales smaller than the forcing scale, where the energy flux degenerates, and to find out what physical mechanism replaces the energy cascade. Computation of fluxes at different strengths of the magnetic field would reveal whether the energy flux is gradually replaced with the enstrophy or helicity flux in the normal plane. Gradual transition to the passive scalar dynamics, expected for the parallel velocity component, and the source of its energy are studied. Comparison with known 2D results, such as spectral powers, amplitudes, dimensionless coefficients, and possible logarithmic corrections is also conducted.

The QNSE theory predicts that with increasing magnetic field strength, the range of scales affected by the field will extend to smaller scales (in agreement with theoretical prediction [14] and experimental results [22,51]), but to clearly see the field effect at large Re , higher resolution is needed. For this reason, instead of going to very high, computationally prohibited resolutions, we chose to extend the inertial range of the turbulence by utilizing analytically derived two-parametric subgrid-scale parametrization [52]. Derivation and testing of the two-parametric viscosity are given in Sec. IV.

II. GOVERNING QUASISTATIC MHD EQUATIONS AND RESULTS OF QNSE ANALYSES

We consider a fully 3D, incompressible, homogeneous MHD turbulent flow with a small Re_m . The fluid is characterized by kinematic viscosity ν_0 , density ρ , electric conductivity σ , magnetic permeability μ , and magnetic diffusivity $\kappa = (\sigma\mu)^{-1}$. The flow is exposed to a permanent uniform magnetic field in the vertical direction, $\mathbf{B} = (0, 0, B)$. The turbulent motion of a conducting fluid inside a magnetic field induces electric currents, which, in turn, generate an additional magnetic field. The magnetic diffusivity causes dissipation of the induced magnetic field. The typical timescale of this effect is $\tau_m = l_0^2/\kappa$, where l_0 denotes the characteristic length scale of the flow. The magnetic Reynolds number $\text{Re}_m = u_0 l_0/\kappa$ is the ratio between τ_m and the large-scale eddy turnover time $\tau_{\text{tu}} = l_0/u_0$, where u_0 is the characteristic velocity of large-scale fluctuations. The assumption of a small Re_m means that the diffusion term in the magnetic induction equation overcomes the convection term. Under this assumption, the induced magnetic field is small in comparison with the applied magnetic field and can be kept only in the diffusion term. The Lorentz force in the hydrodynamic momentum equation reduces to Joule dissipation in the direction of the magnetic field [4] with a characteristic dissipation time of $\tau_J = \rho/(\sigma B^2)$. Finally, the dynamics of the MHD

flow is governed by the QS-MHD equation:

$$\frac{\partial \mathbf{u}}{\partial t} + (\mathbf{u} \cdot \nabla \mathbf{u}) = -\nabla P - \frac{\Delta^{-1}}{\tau_J} \frac{\partial^2 \mathbf{u}}{\partial x_3^2} + \nu_0 \Delta \mathbf{u}, \quad (1)$$

where P is the pressure divided by the constant density, and Δ^{-1} is the inverse Laplacian operator.

When a sufficiently strong magnetic field is applied, the turbulence becomes anisotropic and tends to become two dimensional (in the plane perpendicular to the field) due to Joule damping. Nonlinear interactions disrupt this process by transferring energy between the Fourier modes in an attempt to restore isotropy. The parameter governing this process is the interaction parameter, $N_0 = \tau_{\text{tu}}/\tau_J$, which characterizes the relative strengths between the Joule dissipation and the nonlinear effects. The effect of the Joule dissipation term on the velocity fluctuations can be clearly seen in Fourier space, where the diffusion coefficient in front of this term converts to $1/(\tau_J k^2)$. Thus, while τ_J is scale independent, the dissipation strength decreases with decreasing scales. The relative strength of the Joule dissipation at any given Fourier mode is characterized by the scale-dependent interaction parameter $N(k) = \tau_{\text{tu}}(k)/\tau_J$. The turnover time of a mode k , $\tau_{\text{tu}}(k)$, can be computed using the kinetic energy spectrum $E(k)$, as $\tau_{\text{tu}}(k) = (k^3 E(k))^{-1/2}$, which shows that, for a spectrum shallower than k^{-3} , $N(k)$ decreases with increasing k . It is reasonable to expect that scales with $N(k) > 1$ are strongly affected by the magnetic field, while those with $N(k) < 1$ are weakly affected and remain nearly isotropic. A transitional wave number k_{tr} that separates these domains is located in a region where $N(k) \approx 1$. It has been shown experimentally that in strong magnetic fields the spectrum of liquid-metal MHD turbulence scales as k^{-3} [3,6,53] or even steeper [13] at wave numbers larger than the forcing wave number. At these scales, the local interaction parameter is not decreasing, and thus a transitional wave number would not exist. Nonetheless, several open questions remain: Is there a transitional wave number at weak fields and how does it depend on the magnetic field strength? Can the Kolmogorov $k^{-5/3}$ spectrum at $k > k_{\text{tr}}$ coexist with a steeper MHD spectrum at smaller wave numbers? What would be the spectral power of such a spectrum? The answers to these questions are given by the QNSE analyses of QS-MHD turbulence [37].

According to the QNSE results, the 3D energy spectrum in a weak magnetic field is

$$E(k) = C_K \varepsilon^{2/3} k^{-5/3} [1 + 0.97(k/k_J)^{-2/3}], \quad (2)$$

where $k_J = 1/\sqrt{\tau_J^3 \varepsilon}$ is the wave number at which the Joule dissipation time is comparable with the eddy turnover time, ε is the viscous energy dissipation rate, and $C_K \approx 1.6$ is the Kolmogorov constant. Thus, the first-order correction to the Kolmogorov spectrum is proportional to $k^{-7/3}$. The next-order correction, which becomes dominant at a stronger magnetic field, is proportional to k^{-3} . The magnetic field causes turbulence anisotropization, but the 3D spectrum provides only limited information on the magnetic field effect. A better description of the anisotropy is given by the 1D longitudinal and transverse energy spectra. In a weak magnetic field, the 1D spectra obtained from the QNSE are [37]

$$\begin{aligned} E_1(k_1) &= \frac{18}{55} C_K \varepsilon^{2/3} k_1^{-5/3} [1 + 0.66(k_1/k_J)^{-2/3}] \\ E_1(k_2) &= \frac{24}{55} C_K \varepsilon^{2/3} k_2^{-5/3} [1 + 0.99(k_2/k_J)^{-2/3}] \\ E_1(k_3) &= \frac{24}{55} C_K \varepsilon^{2/3} k_3^{-5/3} [1 + 0.41(k_3/k_J)^{-2/3}], \\ E_3(k_1) &= \frac{24}{55} C_K \varepsilon^{2/3} k_1^{-5/3} [1 + 0.8(k_1/k_J)^{-2/3}] \\ E_3(k_3) &= \frac{18}{55} C_K \varepsilon^{2/3} k_3^{-5/3} [1 + 0.43(k_3/k_J)^{-2/3}] \end{aligned} \quad (3)$$

where $E_i(k_j)$ is the 1D spectrum of the velocity component u_i as a function of k_j . A simple way to estimate the transitional wave number is to equate the Kolmogorov part of the spectrum with the MHD-induced $k^{-7/3}$ part. The result varies from $k_{\text{tr}} \approx k_J$ to $k_{\text{tr}} \approx 3k_J$, depending on the particular 3D or 1D spectrum used for this purpose. Both k_J and k_{tr} are proportional to $B^3 \varepsilon^{-1/2}$. These analytical predictions were compared with the results of DNS, as detailed below.

III. DETAILS OF THE DNS SCHEME

QS-MHD equation (1) was solved using a pseudospectral code in a cubic box with up to 1024^3 grid points. The numerical scheme was similar to that used by Gotoh *et al.* [54]. The pressure term was eliminated by using the continuity equation, with the following result:

$$\left(\frac{\partial}{\partial t} + \nu_0 k^2 + \frac{\sigma B^2 k_3^2}{\rho k^2}\right) u_i(\mathbf{k}) = P_{ij}(\mathbf{k}) \mathcal{F}[\mathbf{u} \times \boldsymbol{\zeta}]_j(\mathbf{k}) + \xi_i(\mathbf{k}), \quad (4)$$

where $\boldsymbol{\zeta}$ is the vorticity field, $P_{ij}(\mathbf{k})$ is the projection operator on the plane normal to \mathbf{k} , and \mathcal{F} is the Fourier transform operator. The forcing term $\xi_i(\mathbf{k})$ maintains the turbulence in a statistically steady state. It is a solenoidal, white in time, Gaussian random force with the correlator

$$\langle \xi_i(t, \mathbf{k}) \xi_j(t', -\mathbf{k}) \rangle = P_{ij}(\mathbf{k}) \frac{F(k)}{4\pi k^2} \delta(t - t'). \quad (5)$$

The forcing spectrum $F(k)$ is constant over the low wave-number band, and zero otherwise. The force is normalized as

$$\int_0^\infty F(k) dk = \varepsilon_{\text{inj}}. \quad (6)$$

In all simulations, the forcing was placed in the range $1 \leq k \leq \sqrt{6}$ and kept constant. The value of ε_{inj} was chosen to be 0.5 at a resolution of 1024^3 and $B = 0$, for testing by comparison with Ref. [54]. All linear terms in Eq. (4) were computed in Fourier space, whereas the nonlinear term, $\mathbf{u} \times \boldsymbol{\zeta}$, was computed in physical space and then Fourier transformed. Periodic boundary conditions were applied in all three directions. The fourth-order Runge-Kutta-Gill method was employed for the time stepping. To reduce the computational time, the initial condition was taken from a fully developed lower-resolution result interpolated to a high-resolution grid. To remove the aliasing error, we used a truncation method [55] with $k_{\text{max}} = \sqrt{2}n/3$, where n^3 is the total number of grid points. At the highest (viscous) end of the spectrum, the condition $k_{\text{max}}/k_{\text{diss}} > 1$ was satisfied, where $k_{\text{diss}} = (\varepsilon/\nu_0^3)^{1/4}$ is the Kolmogorov dissipation wave number. A maximal Taylor microscale Reynolds number of $\text{Re}_\lambda = 407$ was achieved in the nonmagnetic simulations. After the steady state was reached, all the computed quantities were averaged in time. Additional details of the numerical scheme can be found in Gotoh *et al.* [54].

The computed quantities include the total turbulent energy

$$\frac{3}{2} U^2 = \frac{1}{2} \langle u_i \cdot u_i \rangle = E = \int_0^\infty E(k) dk, \quad (7)$$

the viscous energy dissipation rate

$$\varepsilon = 2\nu_0 \int_0^\infty k^2 E(k) dk, \quad (8)$$

and the rate of energy dissipation by magnetic friction

$$\varepsilon_J = \tau_J^{-1} \left\langle \iiint |\mathbf{u}(\mathbf{k})|^2 \frac{k_3^2}{k^2} \frac{d\mathbf{k}}{(2\pi)^3} \right\rangle. \quad (9)$$

Three-dimensional and different 1D spectra, energy and enstrophy fluxes, and other parameters will be defined later.

The large-scale interaction parameter $N_0 = \tau_{\text{tu}}/\tau_J$ was computed using the following estimation of the large-scale eddy turnover time:

$$\tau_{\text{tu}} = (L_0^2/\varepsilon_{\text{inj}})^{1/3}, \quad (10)$$

TABLE I. Parameters of the simulations.

n	N_0	R_0	τ_J^{-1}	ν_0	ε_{inj}	ε
512^3	0	1 770	0	6×10^{-4}	0.44	0.44
512^3	1.5	1 870	1	6×10^{-4}	0.52	8.5×10^{-2}
512^3	9.4	1 750	6	6×10^{-4}	0.43	2.6×10^{-2}
512^3	16	1 740	10	6×10^{-4}	0.42	5×10^{-2}
512^3	62	1 770	40	6×10^{-4}	0.44	7.4×10^{-2}
512^3	95	1 730	60	6×10^{-4}	0.41	7.3×10^{-2}
512^3	127	1 730	80	6×10^{-4}	0.41	8×10^{-2}
512^3	254	1 730	160	6×10^{-4}	0.41	8.8×10^{-2}
1024^3	0	3 950	0	2.8×10^{-4}	0.5	0.5
1024^3	1.5	3 840	1	2.8×10^{-4}	0.46	6.4×10^{-2}
1024^3	4.9	10 000	3	1×10^{-4}	0.37	9.6×10^{-3}
1024^3	252	5 220	160	2×10^{-4}	0.42	7.7×10^{-2}
1024^3	806	5 100	500	2×10^{-4}	0.39	7.2×10^{-2}
1024^3	0		0	TPEV	0.6	0.6
1024^3	1.5		1	TPEV	0.54	7.7×10^{-2}
1024^3	2.2		1.5	TPEV	0.52	4×10^{-2}

where $L_0 = \pi/k_f$, ε_{inj} and k_f are the total energy injection rate and the forcing wave number, respectively. The forcing wave number $k_f = \sqrt{6}$ was set at the end of the forcing range. The energy injection rate was computed using the energy balance equation:

$$\varepsilon_{\text{inj}} = \varepsilon + \varepsilon_J. \quad (11)$$

Computations with a weak magnetic field were used to examine the effect of the magnetic field strength on the progressive turbulence anisotropization and to validate the QNSE predictions. The parameters and the computed physical quantities of the simulations are summarized in Table I. The runs are completely characterized by two dimensionless parameters presented in the table: N_0 and $R_0 = \tau_v/\tau_{\text{tu}}$, where the ‘‘viscous dissipation’’ time τ_v was defined as

$$\tau_v = L_0^2/\nu_0. \quad (12)$$

R_0 was chosen instead of the microscale Reynolds number Re_λ due to ambiguity in definition of the microscale caused by the flow anisotropy. Dimensional parameters (Joule time, viscosity, and energy injection rate) are shown in the table to make it easier to reproduce our results and for verification of scaling dependences of spectra on energy, enstrophy, or helicity fluxes. There are only two basic units in this problem: length L and time T . The units of viscosity and energy flux are L^2/T and L^2/T^3 , respectively. The length of the box is 2π , which defines the unit of length. The unit of time is defined by the value of $\varepsilon_{\text{inj}} = 0.5$ at $B = 0$.

The highest resolution in this study, 1024^3 , was not sufficient to clearly reveal the transition from the $k^{-7/3}$ to the $k^{-5/3}$ part of the spectrum. Thus, the two-parametric eddy viscosity (TPEV) $\nu(k|k_c)$, defined in the next section, was employed to extend the Kolmogorov inertial range.

IV. TWO-PARAMETRIC EDDY VISCOSITY

Kraichnan, in his noted paper [52], clarified the limitations on the use of the customary eddy viscosity to represent the dynamic effects of small-scale turbulence. The classical concept of eddy viscosity implies that small scales act on other scales as if to augment the impact of thermal molecular motion. The effect of thermal agitation is represented by a molecular viscosity, which

is independent of the fluid motion due to the large separation between the spatial and temporal scales of molecular and fluid motions. The analogy between subgrid scales of turbulence and thermal agitation is flawed because turbulence displays a continuous distribution of scale sizes, with no separation between subgrid and resolvable scales. Kraichnan explained that the correct representation of the effect of scales with $k > k_c$ on any mode $k < k_c$ should account for the energy transfer $T(k|k_c)$ from mode k to all modes $k > k_c$. Then, an effective eddy viscosity, acting on a mode k due to dynamic interactions with subgrid scales $k > k_c$, may be defined by

$$\nu(k|k_c) = -T(k|k_c)/[2k^2 E(k)], \quad (13)$$

with the energy-transfer function $T(k|k_c)$ given by the integral of the triad $(\mathbf{k}, \mathbf{p}, \mathbf{q})$ interactions

$$T(k|k_c) = \iint_{\Delta} T(k, p, q) dp dq, \quad k < k_c, \quad (14)$$

where

$$T(k, p, q) = -\frac{i}{2} P_{\alpha\beta\gamma}(\mathbf{k}) \langle u_{\alpha}(-\mathbf{k}) u_{\beta}(\mathbf{p}) u_{\gamma}(\mathbf{q}) \rangle \quad (15)$$

and the integral \iint_{Δ} is taken over all the wave-number triads $\mathbf{k} + \mathbf{p} + \mathbf{q} = 0$ with p and/or $q > k_c$. For isotropic 3D or 2D turbulence, the energy transfer function $T(k|k_c)$ can be computed using one of the quasinormal approximations [56]. In the 3D case, the function $T(k, p, q)$ is given by

$$T(k, p, q) = 4\pi^2 k^3 b_3(k, p, q) p q \theta_{k,p,q} [U(p) - U(k)] U(q), \quad (16)$$

in which

$$b_3(k, p, q) = \frac{1}{2} k^{-4} \sin^2 \alpha [(k^2 - q^2)(p^2 - q^2 + k^2 p^2)], \quad (17)$$

where α is the angle opposite k in the triad (k, p, q) and $\theta_{k,p,q}$ is the characteristic time of the triad interaction. The latter can be determined by using the QNSE-derived eddy viscosity $\nu_n(k)$ (A8) as

$$\theta_{k,p,q} = [\nu_n(k)k^2 + \nu_n(p)p^2 + \nu_n(q)q^2]^{-1}. \quad (18)$$

This result was first obtained by Dannevik *et al.* [57] employing the renormalization group (RNG) theory. It was adapted for 2D isotropic and anisotropic turbulence in Refs. [58] and [59], respectively.

The analytically derived TPEV $\nu(k|k_c)$ was tested by DNS. The velocity field was computed by solving Eq. (4) with $B = 0$ using 1024^3 Fourier modes. Next, we calculated the energy-transfer function $T(k|k_c)$ by computing the third-order velocity cumulant (15) from the DNS results and substituting it into the integral (14). We set $k_c = 50$ well inside the inertial subrange. The DNS-inferred normalized TPEV $\nu(k|k_c)/\nu(0|k_c)$ is plotted in Fig. 1(a), along with the QNSE-based analytical prediction. A similar comparison of the DNS and the analytical TPEV in two dimensions taken from Ref. [58] is plotted in Fig. 1(b). The agreement between the DNS-based and the analytical results is good up to the wave numbers close to k_c , where the DNS data saturate, while the analytical curves exhibit a sharp cusp. The physics underlying this cusp was explained by Chekhlov *et al.* [58] as follows: the closer k approaches to k_c , the more elongated triads, with either p or $q \ll k_c$, become involved in the energy exchange between the mode k and the subgrid-scale modes. The contribution from triads with small p or q brings about the cusp behavior of the theoretical TPEV. In a finite box DNS, the energy of small wave-number modes is low. As a result, instead of growing sharply, the TPEV saturates as k approaches k_c . This effect decreases as the cutoff wave number k_c increases,

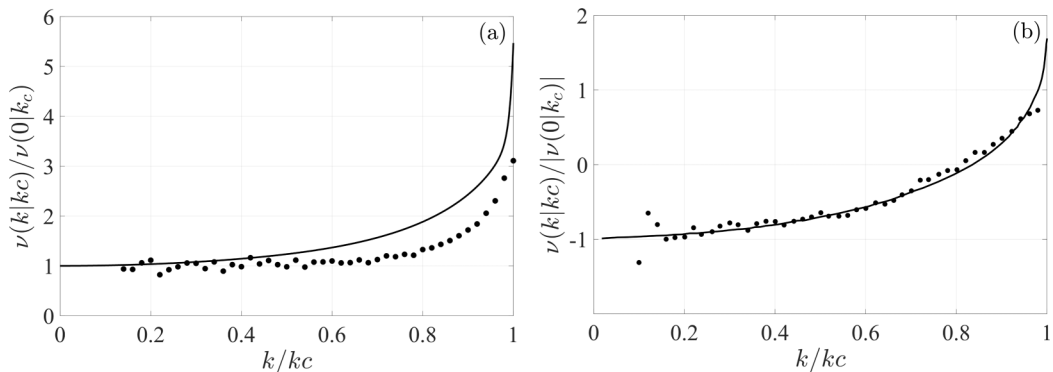


FIG. 1. Two-parametric viscosity $\nu(k|k_c)$ normalized by $\nu(0|k_c)$ for 3D geometry (left panel) and 2D geometry (right panel). The 2D results are taken from Ref. [58]. The solid line represents theoretical curves, and the dots are the DNS results.

and the TPEV approaches the theoretical curve, as was verified by the DNS with k_c set to 20, 30, and 40 (not shown here).

Finally, we ran 1024^3 -resolution simulations with the TPEV in which k_c was set to 483, the maximal resolvable wave number after the de-aliasing truncation. The ratio of k_c to the Kolmogorov dissipation wave number for the DNS, k_c/k_{diss} , equals 1.26. The energy spectrum shown in Fig. 2(a) exhibits almost perfect $-5/3$ scaling over a wide range of scales. In simulations with constant viscosity, the Kolmogorov inertial range extends from the forcing scale to $k \approx 25$, and it increases by more than twofold when the TPEV is employed. A bulge typical of the near-dissipation region of the energy cascade range appears at the high wave-numbers end of the spectrum [60–62]. The compensated spectrum presented in Fig. 2(b) shows the Kolmogorov constant $C_K \approx 1.6$, which is in the range of 1.62 ± 0.17 that was established in Ref. [63], based upon numerous experiments and observations.

Summarizing, TPEV emulates the dynamic effects of subgrid scales (SGS) on the resolvable scales without distorting them and without disrupting the downscale energy cascade. The use of TPEV as the SGS representation allows for extension of the inertial range up to the largest resolvable wave number k_c .

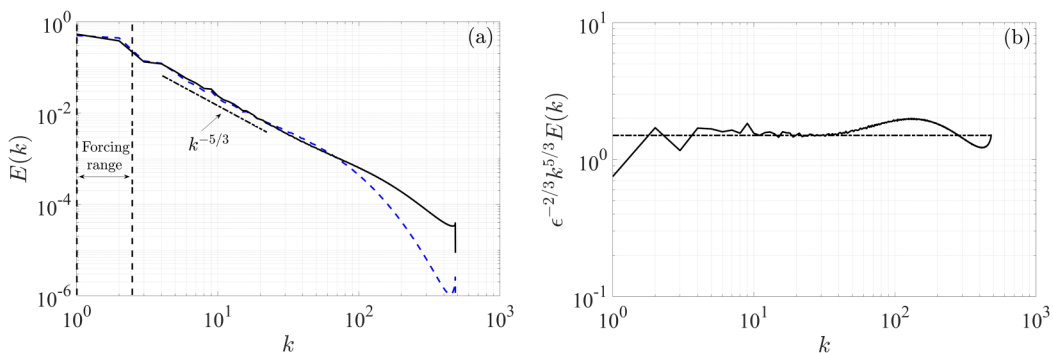


FIG. 2. (a) The 3D energy spectrum in 1024^3 grid-point simulations with constant viscosity ($R_0 = 3950$, dashed blue line) and TPEV (solid black line); (b) compensated energy spectrum obtained with TPEV.

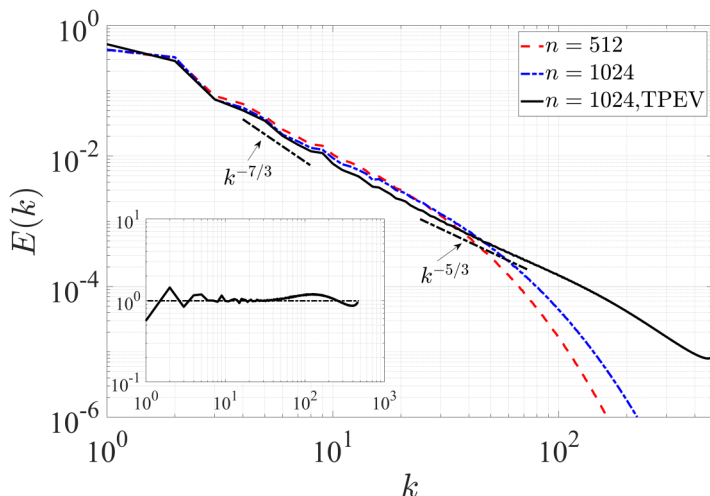


FIG. 3. The 3D energy spectrum at $N_0 = 1.5$ computed with constant viscosity and TPEV. Dashed red and dashed-dotted blue lines correspond to DNS with resolutions 512^3 and 1024^3 ($R_0 = 1870$ and 3840), respectively. The solid black line corresponds to results with TPEV. The spectrum obtained with TPEV, divided by the theoretical prediction (2), is shown in the inset.

V. VERIFICATION OF THE QNSE RESULTS BY USING DNS

A. Modification of the energy spectra by a weak magnetic field

The results presented in the previous section indicate that the TPEV is an efficient device, allowing maximal extension of the inertial range up to the highest resolvable wave number, which is effectively equivalent to increasing the Reynolds number. This extension is important for identification of different slopes in the kinetic energy spectrum, as predicted by the QNSE theory, namely, the $-7/3$ slope, imposed by the magnetic field effect at the lower end of the spectrum, and the residual Kolmogorov $-5/3$ slope at the higher end of the inertial range.

Modification of the spectrum $E(k)$ by a relatively weak magnetic field ($N_0 = 1.5$) is presented in Fig. 3 for simulations with 512^3 and 1024^3 grid points. The $-7/3$ power law is clearly seen at low wave numbers. As the magnetic field increases, the $-7/3$ range propagates toward higher wave numbers, where it changes to the $-5/3$ power law. A relatively short inertial range in simulations with constant (“molecular”) viscosity makes it difficult to conclusively identify the transition. Only at the highest resolution is the transition from the $k^{-7/3}$ to the $k^{-5/3}$ spectrum evident. The transition is clearly seen in the simulations with 1024^3 grid points and TPEV. In this case the ratio between the computed spectrum and the QNSE prediction (2) at $N_0 = 1.5$ is very close to 1.

It is important to evaluate the extension of the spectral region affected by the magnetic field and to determine the boundary of the $-7/3$ spectral range propagation toward higher wave numbers with increasing field strength. Figure 4 shows the 3D energy spectra obtained in simulations with 1024^3 grid points and with either the TPEV [Fig. 4(a)] or constant viscosity [Fig. 4(b)]. The spectra shown in Fig. 4(a) correspond to three different values of the interaction parameter, $N_0 = 0$, $N_0 = 1.5$, and $N_0 = 2.2$, while the spectrum in Fig. 4(b) corresponds to $N_0 = 4.9$. The two slopes exist in nonzero field simulations with TPEV. The transitional wave number moves from $k_{tr} \approx 10$ at $N_0 = 1.5$ to $k_{tr} \approx 15$ at $N_0 = 2.2$. With an increasing field, at $N_0 = 4.9$ the $-7/3$ power law extends to the whole range of scales not affected by viscous dissipation, as may be seen in Fig. 4(b). At such a field strength, the isotropic equations (16)–(18) are not valid for computations of two-parametric viscosity, and therefore constant viscosity was used in the DNS. The computed value of k_J is 53, indicating that the transition occurs inside the dissipation range and cannot be seen on the spectrum.

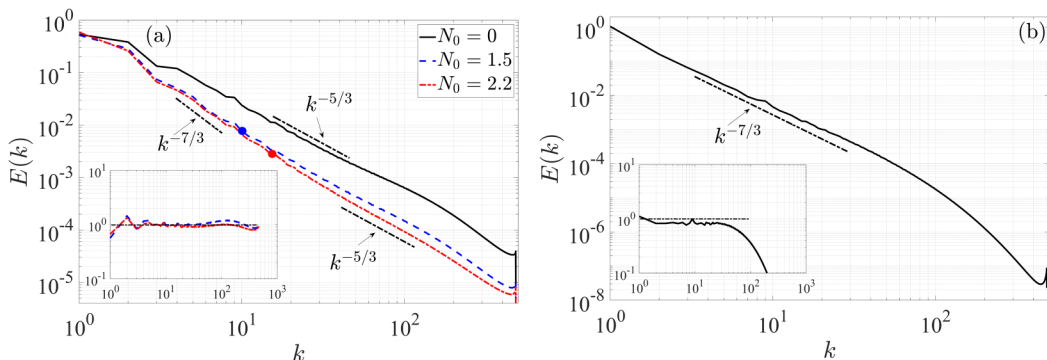


FIG. 4. The 3D energy spectra for different values of the interaction parameter (a) $N_0 = 0$ (black solid line), 1.5 (dashed blue line), and 2.2 (red dashed-dotted line), TPEV and (b) $N_0 = 4.9$, $R_0 = 10000$, DNS. The spectra compensated by the QNSE prediction (2) are shown in the insets.

The theoretical scaling is further verified in the next section where the ratios between the numerical and theoretical spectra are presented.

B. Detailed comparison of DNS with the QNSE theory: 3D and 1D spectra

The QNSE theory not only predicts development of the $-7/3$ power scaling spectral range and its propagation to higher wave numbers with an increasing magnetic field, but also determines the spectral amplitudes. The QNSE-derived spectra were verified by comparison with the results of numerical simulations. Figures 5(a)–5(f) show 3D and 1D energy spectra at various strengths of the magnetic field, divided by the corresponding theoretical spectra (2) and (3). At the relatively small interaction parameters, $N_0 = 1.5$ and $N_0 = 2.2$, these ratios are close to 1 over the whole range of resolvable scales, with the exception of the near-dissipation cutoff region. In that region, the 3D spectrum exhibits the foreseen “bump,” while the 1D spectra decay quickly. This decay may be explained by the use of the TPEV, which was designed to emulate the dissipative effect of all scales $k > k_c$, while the theoretical 1D spectra $E_i(k_j)$ contain contributions from wave vectors \mathbf{k} whose amplitude is larger than k_c [recall that $E_i(k_j)$ is computed by integration of $|u_i(\mathbf{k})|^2$ over the plane orthogonal to the j axis [37]]. The good agreement obtained between the theoretical 1D spectra and the DNS results is especially important, since 1D spectra provide detailed information on the development of anisotropy due to the impact of the magnetic field.

At a stronger field, $N_0 = 4.9$, constant viscosity was used, and the scales with $k > 30$ were suppressed by viscous dissipation. On larger, not suppressed, scales, the agreement of the 3D spectrum $E(k)$ and 1D spectrum $E_3(k_3)$ with the QNSE theory remains good, but all other 1D theoretical spectra, except the transverse spectrum of the velocity component parallel to the field, $E_3(k_1)$, are greater than the DNS spectra. Recall that the QNSE theory was developed on the assumption of a weak magnetic field. The DNS results determine the limit of this approximation, which is valid at least up to $N_0 = 2.2$, but becomes inaccurate at $N_0 > 4$.

VI. QS-MHD TURBULENCE IN INTERMEDIATE AND STRONG MAGNETIC FIELDS: TRANSITION TO QUASI-2D TURBULENCE

Since the application of the QNSE theory to QS-MHD, which is based on a weak magnetic field approximation, is inaccurate at $N_0 > 4$, the turbulence anisotropization at stronger fields was studied numerically. DNSs were performed with a progressively increasing interaction parameter whose value was set to 9.4, 16, 62, 95, 127, and 254. To save run time, the simulations in this range were performed with 512^3 grid points and $R_0 \approx 1750$. Modification of the 3D spectrum with an

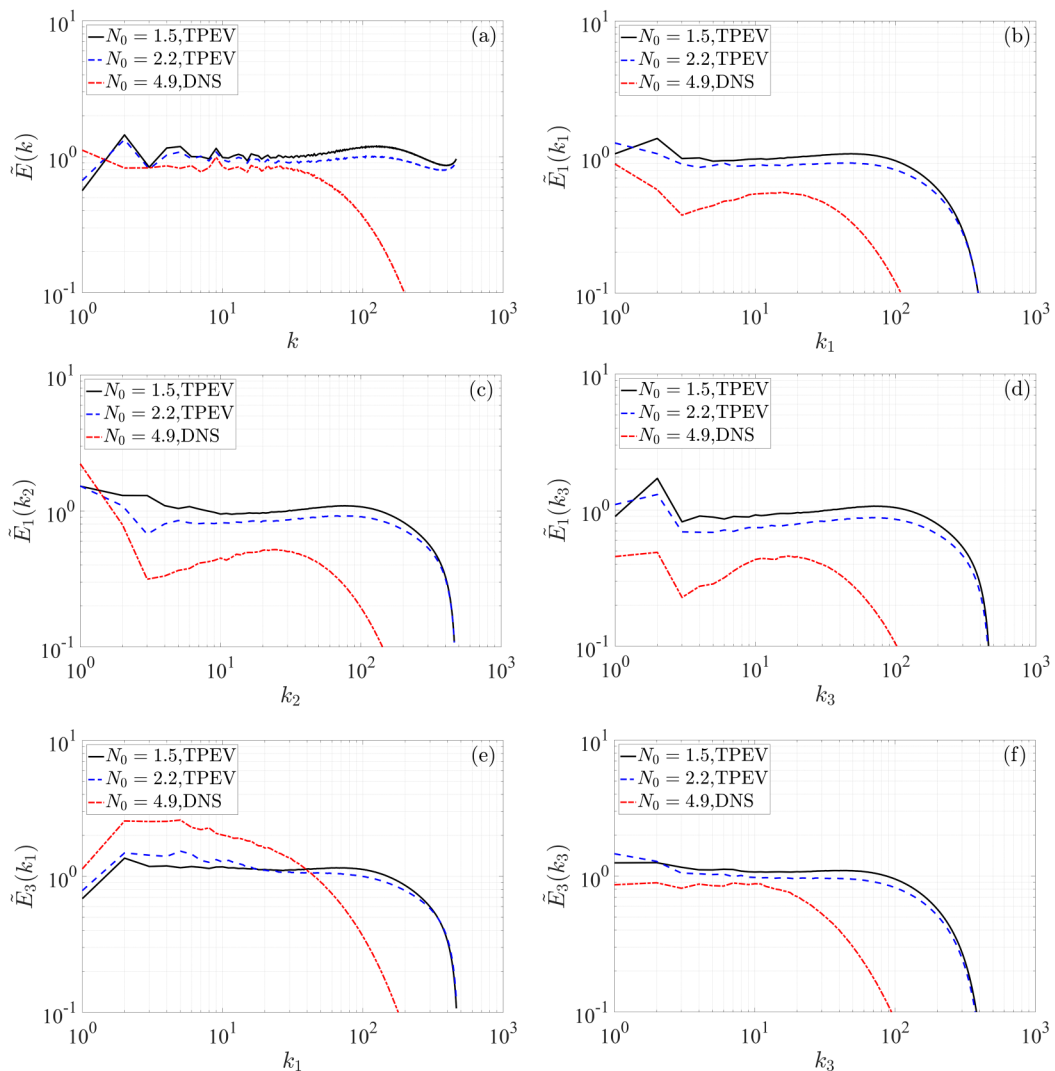


FIG. 5. Energy spectra normalized by the QNSE prediction: (a) normalized 3D spectrum $\tilde{E}(k) = E(k)/E(k)_{\text{QNSE}}$; (b)–(f) normalized 1D spectra $\tilde{E}_i(k_j) = E_i(k_j)/E_i(k_j)_{\text{QNSE}}$. Solid black, dashed blue, and dashed-dotted red lines correspond to $N_0 = 1.5$, $N_0 = 2.2$, TPEV and $N_0 = 4.9$, $R_0 = 10000$, DNS, respectively.

increasing field is shown in Fig. 6. At $N_0 = 9.4$, the spectrum still obeys the $-7/3$ power law. This scaling disappears with increasing field strength, and the spectrum becomes shallower.

Due to turbulence anisotropy in a strong magnetic field, the 3D spectrum becomes less informative as it mixes energies of parallel and perpendicular flow components and scale directions. In addition, Fig. 6 indicates that it is doubtful whether $E(k)$ obeys a universal scaling. The 1D and 2D spectra are far more informative, since they shed light on the turbulence anisotropization and the modification of turbulence dynamics. The modification of the transverse and longitudinal 1D spectra, $E_1(k_3)$ and $E_3(k_3)$, with an increasing magnetic field is shown in Fig. 7. As expected, the fluctuations in the direction of the magnetic field (k_3) degenerate as the interaction parameter increases. All scales are suppressed by several orders of magnitude, with the smallest scales being completely smoothed out.

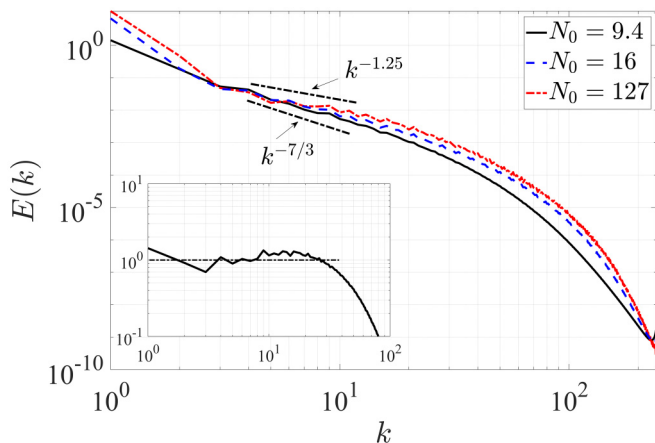


FIG. 6. The 3D energy spectra at different magnetic field strengths: $N_0 = 9.4$, solid black line; $N_0 = 16$ dashed blue line; $N_0 = 127$ dashed-dotted red line. The spectrum at $N_0 = 9.4$ compensated by $k^{-7/3}$ is shown in the inset.

Most interesting are the 2D energy spectra of the velocity field in the plane normal to \mathbf{B} ,

$$E_{\perp}(k_{\perp}) = 1/2 \iint_{S(k_{\perp})} \langle |u_1(\mathbf{k})|^2 + |u_2(\mathbf{k})|^2 \rangle \frac{d\sigma}{(2\pi)^3} \quad (19)$$

and the velocity component parallel to \mathbf{B} ,

$$E_{\parallel}(k_{\perp}) = 1/2 \iint_{S(k_{\perp})} \langle |u_3(\mathbf{k})|^2 \rangle \frac{d\sigma}{(2\pi)^3} \quad (20)$$

as functions of the perpendicular wave number $k_{\perp} = \sqrt{k_1^2 + k_2^2}$. Here $S(k_{\perp})$ is a cylindrical shell of radius k_{\perp} . With increasing magnetic field strength, these spectra undergo significant changes, indicating a transition to quasi-2D turbulence. Spectra $E_{\perp}(k_{\perp})$ and $E_{\parallel}(k_{\perp})$ at intermediate values of N_0 are shown in Figs. 8(a) and 8(b), respectively. Both spectra obey the $-7/3$ scaling power law at $N_0 = 9.4$ between the forcing and viscous dissipation ranges. The perpendicular spectrum $E_{\perp}(k_{\perp})$ almost does not change with increasing N_0 , and the $-7/3$ power law remains intact up to $N_0 = 62$. In

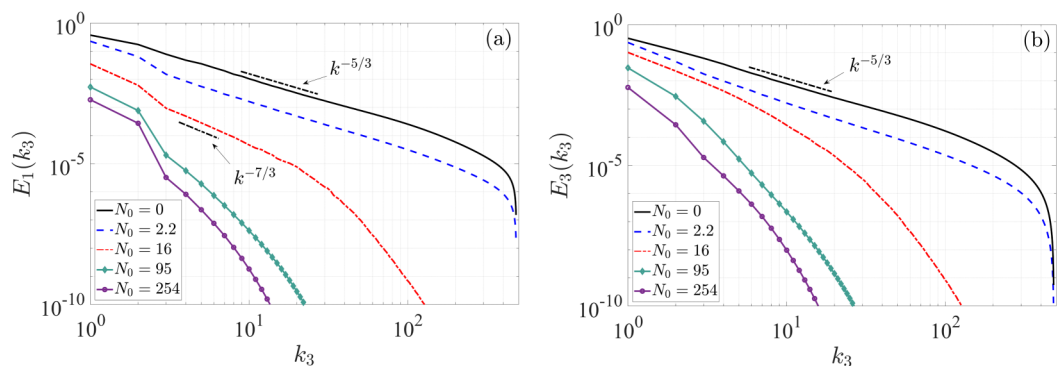


FIG. 7. Modification of the transverse $E_1(k_3)$ and longitudinal $E_3(k_3)$ spectra with an increasing magnetic field.

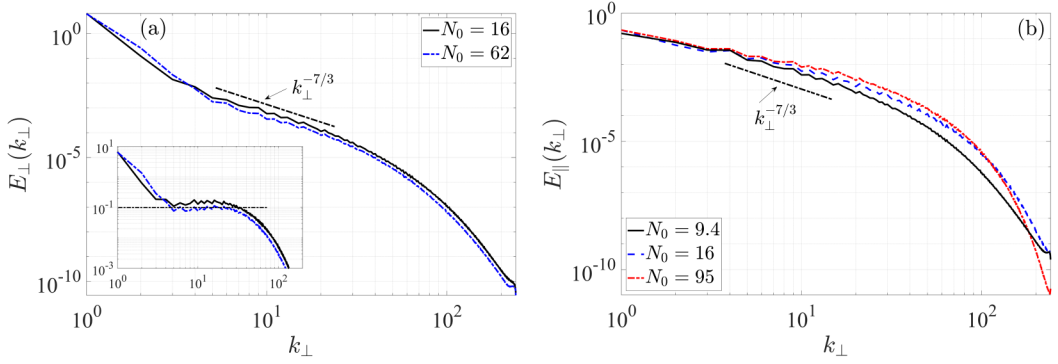


FIG. 8. Perpendicular and parallel energy spectra at intermediate values of the interaction parameter. The perpendicular spectra compensated by $k_{\perp}^{-7/3}$ are shown in the inset.

this range of the interaction parameter and beyond, the parallel spectrum $E_{\parallel}(k_{\perp})$ gradually becomes less steep.

A dramatic change occurs at $N_0 = 95$. At this value of the interaction parameter, the perpendicular spectrum $E_{\perp}(k_{\perp})$ becomes proportional to k^{-3} in a wide range of scales [see Fig. 9(a)], while the parallel spectrum $E_{\parallel}(k_{\perp})$ scales as k^{-1} [Fig. 9(b)]. Both spectra remain unchanged with further increases in the strength of the magnetic field. This lack of sensitivity of the spectra to Joule friction implies that the velocity field has become completely smoothed in the direction of the magnetic field (a claim supported by Fig. 7, which shows that the fluctuations in the field direction are strongly suppressed). In other words, at such interaction parameters, the turbulence reaches the 2D-3C state [26].

We now reexamine the action of Joule friction on turbulence. In a weak magnetic field, the dominant effect of Joule friction is seen in decreasing gradients in the direction of the magnetic field. This, in turn, leads to suppression of nonlinear interactions between the perpendicular and the parallel flow components. Eventually, the parallel component becomes passive scalar steered and advected by the 2D perpendicular flow field [64].

So far we have analyzed spectral powers. The -3 power spectrum in 2D is commonly associated with a direct enstrophy cascade [19,65]. However, QS-MHD is an anisotropic 3D phenomenon, with an additional governing dimensional parameter, τ_J . Although it is known that the spectral slopes in a strong magnetic field correspond to isotropic 2D turbulence, additional information is necessary to

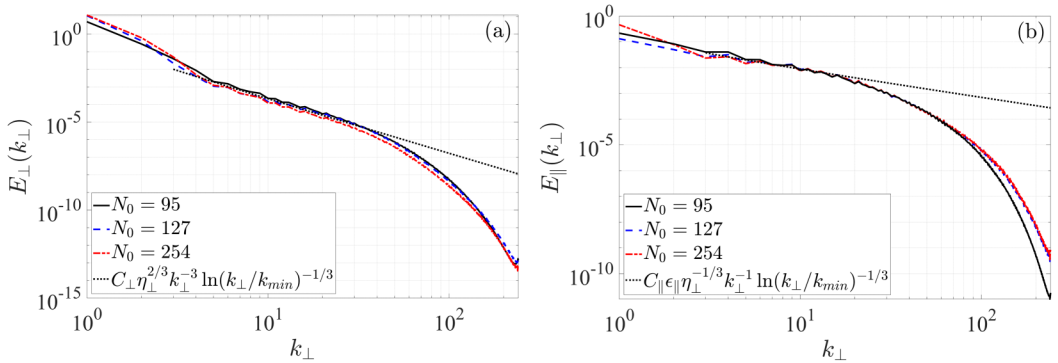


FIG. 9. Perpendicular and parallel energy spectra at large values of the interaction parameter.

clarify the underlying physics. Energy and enstrophy fluxes together with spectral amplitudes will provide the required information.

VII. ENERGY AND ENSTROPY FLUXES

In anisotropic turbulence, the fluxes—also being anisotropic—have to be considered separately for different flow components and in different spectral directions. Most interesting are the fluxes of perpendicular and parallel energy $\Pi_{E\perp}(k_\perp)$, $\Pi_{E\parallel}(k_\perp)$ and enstrophy $\Pi_{Z\perp}(k_\perp)$, $\Pi_{Z\parallel}(k_\perp)$ from the spectral region inside a cylinder of radius k_\perp outward. The flux is negative if it is directed inward. An efficient method for computation of the energy or enstrophy fluxes is to compute the nonlinear term in the corresponding momentum or vorticity equation in physical space, Fourier transform it, and multiply it by filtered velocity or vorticity with all Fourier modes $k_1^2 + k_2^2 > k_\perp^2$ set to 0. The filtered velocity is defined as

$$\mathbf{u}(\mathbf{k}, t|k_\perp) = \mathbf{u}(\mathbf{k}, t) \theta(k_\perp - \sqrt{k_1^2 + k_2^2}), \quad (21)$$

where θ is a Heaviside step function. The real part of the result is integrated over the cylinder and time averaged. To be more precise, the energy fluxes are

$$\Pi_{E\perp}(k_\perp) = -\Re \left\langle \iiint_{V(k_\perp)} u_i^*(\mathbf{k}, t|k_\perp) \mathcal{F} \left(u_j \frac{\partial u_i}{\partial x_j} \right) \frac{d\mathbf{k}}{(2\pi)^3} \right\rangle, \quad i \neq 3, \quad (22)$$

$$\Pi_{E\parallel}(k_\perp) = -\Re \left\langle \iiint_{V(k_\perp)} u_3^*(\mathbf{k}, t|k_\perp) \mathcal{F} \left(u_j \frac{\partial u_3}{\partial x_j} \right) \frac{d\mathbf{k}}{(2\pi)^3} \right\rangle. \quad (23)$$

where the symbols \Re and $*$ denote the real part and the complex conjugate, respectively. The integral is computed over a cylindrical volume of radius k_\perp , $V(k_\perp)$. The summation over repeating indexes is implied, whereas the summation in (22) involves only i equal 1 and 2.

Similar formulas are used for the computation of enstrophy fluxes based on the vorticity equation. Note that the “perpendicular” enstrophy is the mean-square vorticity of the 2D velocity field perpendicular to \mathbf{B} . In other words, if $\boldsymbol{\zeta} = \nabla \times \mathbf{u}$ is vorticity, then $Z_\perp = \langle |\zeta_3|^2 \rangle$:

$$\Pi_{Z\perp}(k_\perp) = -\Re \left\langle \iiint_{V(k_\perp)} \zeta_3^*(\mathbf{k}, t|k_\perp) \mathcal{F} \left(u_j \frac{\partial \zeta_3}{\partial x_j} \right) \frac{d\mathbf{k}}{(2\pi)^3} \right\rangle, \quad (24)$$

$$\Pi_{Z\parallel}(k_\perp) = -\Re \left\langle \iiint_{V(k_\perp)} \zeta_i^*(\mathbf{k}, t|k_\perp) \mathcal{F} \left(u_j \frac{\partial \zeta_i}{\partial x_j} \right) \frac{d\mathbf{k}}{(2\pi)^3} \right\rangle, \quad i \neq 3. \quad (25)$$

Energy and enstrophy fluxes at zero field are shown in Fig. 10. As expected, the energy flux is constant in the inertial range. In this region, the enstrophy fluxes grow proportionally with k^2 . The perpendicular flux $\Pi_{E\perp}(k_\perp)$ is twice as large as the parallel flux $\Pi_{E\parallel}(k_\perp)$.

The fluxes change radically as the magnetic field strength increases, as shown in Fig. 11. The changes are caused partially by Joule friction, which dissipates part of the energy injected into the flow. In a weak magnetic field, $N_0 = 1.5$, the parallel and perpendicular energy fluxes remain closely comparable. Marked anisotropization of the energy flux occurs in stronger fields of $N_0 \geq 9.4$. At these values of the interaction parameter, the flux in the plane normal to \mathbf{B} completely degenerates outside of the energy injection region and becomes negative inside this region. The parallel flux changes more gradually, eventually reaching a constant value ε_\parallel in the “inertial” range between the forcing and dissipation ranges (we expect the parallel flux to exhibit a plateau at higher resolution, even though this is not quite reached in the simulation presented). At first sight, the latter result appears peculiar, but it can be explained in terms of quasi-2D dynamics. We will verify that u_3 becomes a 2D passive scalar and explore the origin of ε_\parallel later, but first, we examine the enstrophy fluxes.

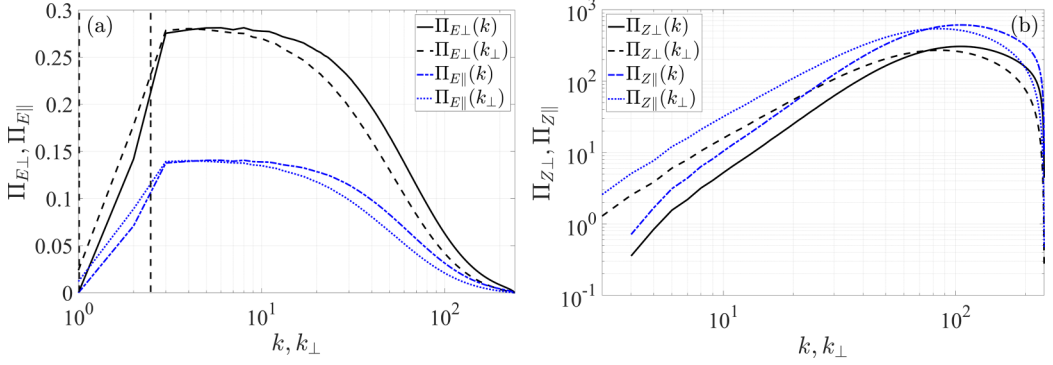


FIG. 10. Perpendicular and parallel components of the energy (a) and enstrophy (b) fluxes at $N_0 = 0$, $R_0 = 1770$. Vertical dashed line shows the energy injection range.

Modification of enstrophy fluxes by a magnetic field is presented in Fig. 12. The parallel flux $\Pi_{Z\parallel}(k_{\perp})$ grows proportionally with k_{\perp}^2 in the region of constant energy flux. The flux in the plane normal to \mathbf{B} , $\Pi_{Z\perp}(k_{\perp})$, decreases with an increasing magnetic field until it levels off at a constant value η_{\perp} in the inertial range at $N_0 \gtrsim 120$. The flux does not change any further at higher values of the interaction parameter. Recall that at such values of N_0 the energy flux in the normal plane is close to 0 and the spectrum $E_{\perp}(k_{\perp})$ is proportional to k_{\perp}^{-3} . A constant-enstrophy flux combined with a zero-energy flux and a -3 power spectrum indicate a direct enstrophy cascade of 2D turbulence. The spectral amplitude provides ultimate evidence of such a cascade.

Kraichnan [66] has shown that the k^{-3} energy spectrum in the enstrophy cascade range should have a logarithmic correction. Using our notations of the 2D spectrum in the normal plane, the corrected form is

$$E_{\perp}(k_{\perp}) = C_{\perp} \eta_{\perp}^{2/3} k_{\perp}^{-3} \ln(k_{\perp}/k_{\min})^{-1/3}, \quad (26)$$

where C_{\perp} is a dimensionless constant, η_{\perp} is the rate of enstrophy transfer, and $k_{\min} = 1$ marks the bottom of the range where energy is injected. Using the mean value of the enstrophy flux in the range $3 \leq k \leq 20$ where $\Pi_{Z\perp}(k_{\perp})$ is nearly constant and dividing the DNS-derived spectrum by theoretical spectrum (26), we found that $1 < C_{\perp} < 1.5$ (see Fig. 18). The Lagrangian renormalized approximation (LRA) model yields $C_{\perp} \simeq 1.44$ [67], which is quite close to our estimate. Gotoh [68] found from DNS that C_{\perp} is of the order of 1 but increases with the microscale Reynolds number. Summarizing all the above results, namely, the good fit of the spectrum $E_{\perp}(k_{\perp})$ to the theoretical

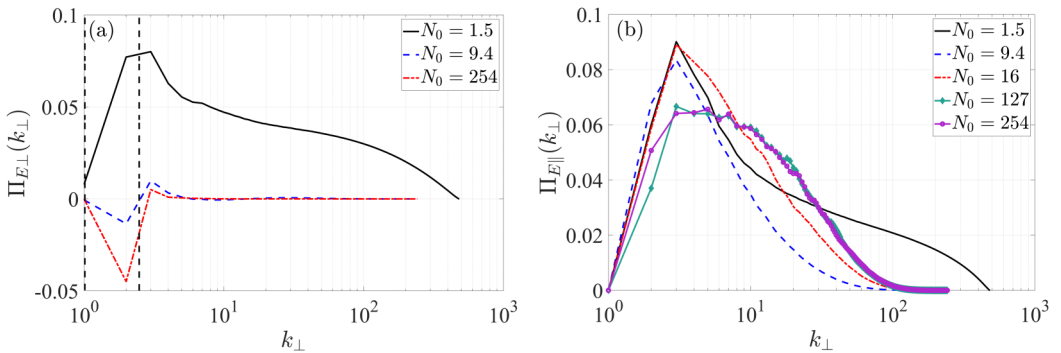


FIG. 11. Modification of perpendicular (a) and parallel (b) components of the energy flux with increasing magnetic field strength. Vertical dashed line shows the energy injection range.

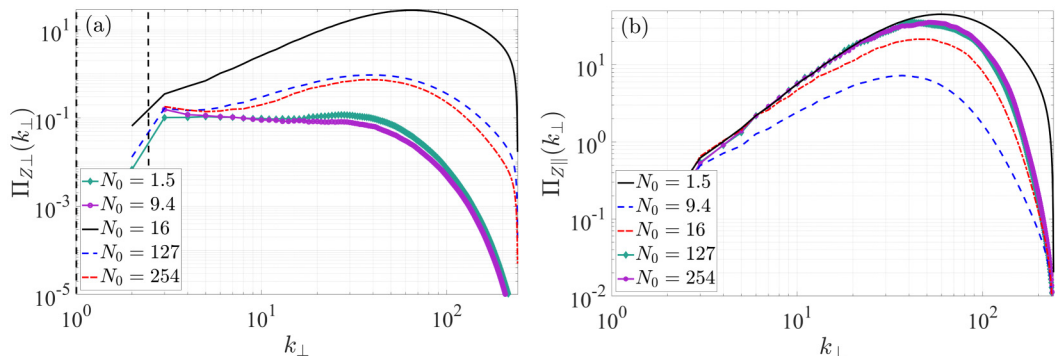


FIG. 12. Perpendicular (a) and parallel (b) components of the enstrophy flux as function of k_{\perp} for the range of the interaction parameter from low, $N_0 = 1.5$, to high, $N_0 = 254$. Vertical dashed line shows the energy injection range.

form (26), correct spectral amplitude, the nearly constant enstrophy flux, and the zero-energy flux in the normal plane, it can be concluded that in a strong field ($N_0 \sim 120$ and higher) the turbulence attains a 2D state.

In the remainder of this section, we verify that the properties of u_3 , the velocity component parallel to \mathbf{B} , are consistent with 2D dynamics. At large N_0 , the turbulent field is almost independent of the vertical coordinate. Consequently, Eq. (1) for u_3 turns into the equation of a passive scalar advected by the perpendicular flow components u_1 and u_2 . It is known that for the enstrophy cascade of 2D turbulence, the spectrum of scalar variance in the inertial-convective range follows a k^{-1} law [69,70]. We compare this spectrum with the 2D energy spectrum of u_3 , $E_{\parallel}(k_{\perp})$, at $N_0 \geq 127$. The theoretical spectrum in our notations is

$$E_{\parallel}(k_{\perp}) = C_{\parallel} \varepsilon_{\parallel} \eta_{\perp}^{-1/3} k_{\perp}^{-1} \ln(k_{\perp}/k_{\min})^{-1/3}, \quad (27)$$

where ε_{\parallel} is the rate of energy flux $\Pi_{E_{\parallel}}(k_{\perp})$ in the range of scales where it is nearly constant [see Fig. 11(b)]. The dimensionless constant $C_{\parallel} \approx 0.85$ (see Fig. 13). The dotted line in Fig. 9(b) corresponds to (27) with this value of C_{\parallel} . Gotoh [70] studied passive scalar diffusion in 2D turbulence using the LRA model and found $C_{\parallel} = 0.561$, a value consistent with our estimate.

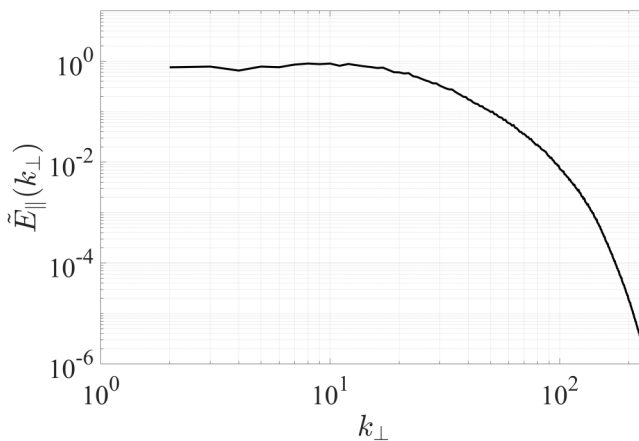


FIG. 13. Compensated energy spectrum $\tilde{E}_{\parallel}(k_{\perp}) = E_{\parallel}(k_{\perp})/(\varepsilon_{\parallel} \eta_{\perp}^{-1/3} k_{\perp}^{-1} \ln(k_{\perp}/k_{\min})^{-1/3})$ at $N_0 = 254$, $R_0 = 1730$.

Our simulations confirm that in a strong magnetic field, turbulent motion in the normal plane corresponds to the 2D enstrophy cascade, while the parallel fluctuations resemble turbulent diffusion of a passive scalar. This resemblance raises questions regarding the energy source for the scalar flux and the mechanism of energy transfer to the parallel velocity component.

VIII. ROLE OF AN EXTERNAL FORCE IN GENERATING THE PARALLEL ENERGY FLUX

Pressure, as a “guardian” of flow incompressibility, causes a redistribution of energy between the velocity components and may thus be a possible source of the parallel energy flux. Another possibility is that there is a direct injection of energy ε_{\parallel} by an external stirring force. The magnitude of the transfer to the parallel component via pressure, $\Pi_{P\parallel}(k_{\perp})$, from the spectral region inside the cylinder of radius k_{\perp} outward, is given by the following integral:

$$\Pi_{P\parallel}(k_{\perp}) = -\Im \left\langle \iiint_{V(k_{\perp})} u_3^*(\mathbf{k}, t) k_3 P(\mathbf{k}, t) \frac{d\mathbf{k}}{(2\pi)^3} \right\rangle, \quad (28)$$

where the symbol \Im designates the imaginary part of the expression. Utilizing the incompressibility equation, the pressure is computed as

$$P(k, t) = \frac{-ik_i}{k^2} \mathcal{F} \left(u_j(\mathbf{x}, t) \frac{\partial u_i(\mathbf{x}, t)}{\partial x_j} \right). \quad (29)$$

Modification of $\Pi_{P\parallel}(k_{\perp})$ by magnetic friction is shown in Fig. 14. Suppression of flow derivatives in the direction of the magnetic field with increasing field strength leads to degeneration of $\Pi_{P\parallel}(k_{\perp})$. In a strong field, $N_0 = 254$, its maximal value is close to 5×10^{-4} , which is smaller than the energy flux $\varepsilon_{\parallel} = 0.065$ by two orders of magnitude. Therefore, the pressure flux cannot be a meaningful source of the energy supplied to the parallel flow component. This leaves a direct injection of energy by an external force as the only possible source of energy.

This result is not surprising, since the equation for u_3 approaches a passive scalar equation not containing pressure as the magnetic field strength increases. A more interesting result is that the turbulent state in a strong field depends on the anisotropy of external forcing and, thus, is not universal. To illustrate this point, we conducted simulations with pure 2D two-component (2D-2C) forcing and 3D two-component (3D-2C) forcing. It is obvious that without any 3D disturbance, the 2D-2C simulations result in a pure 2D turbulent field. Thus, a small-amplitude 3D-2C initial field was generated. Nonmagnetic simulations with 2D-2C forcing quickly evolve into 3D turbulence characterized by an isotropic Kolmogorov $-5/3$ inertial range, independent of the forcing details

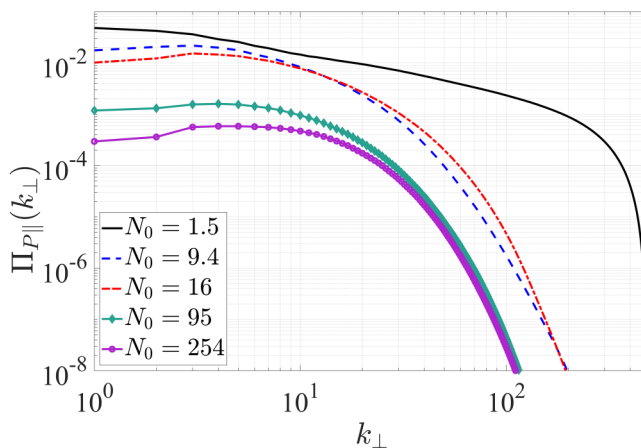


FIG. 14. Modification of the pressure flux $\Pi_{P\parallel}(k_{\perp})$ with increasing magnetic field strength.

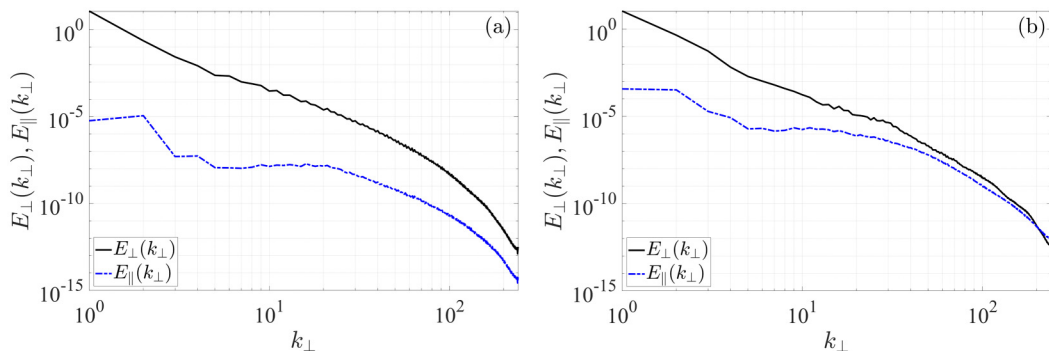


FIG. 15. Perpendicular and parallel energy spectra in simulations with (a) a 2D-2C and (b) a 3D-2C forcing in a strong magnetic field.

and the initial conditions. However, if a strong magnetic field is applied, the simulations result in a quasi-2D turbulent field with a small parallel velocity component that does not adhere to a well-defined power scaling (see Fig. 15).

Comparing the energy spectra shown in Fig. 9 and Fig. 15, we conclude that the perpendicular spectra in 3D-3C, 3D-2C, and 2D-2C simulations are nearly identical, but the parallel spectra in simulations with two-componential forcing are smaller by a few orders of magnitude than those with 3D-3C forcing.

IX. DEPENDENCE ON THE REYNOLDS NUMBER

As shown in the previous section, at large values of the interaction parameter, the flow becomes quasi-2D and turbulence characteristics do not change with further increases of the magnetic field. However, what happens if the interaction parameter is kept constant while the Reynolds number is increased? With increasing R_0 , smaller turbulence scales are excited. These scales may have shorter characteristic times and are thus less susceptible to the anisotropization effect of the Lorentz force. Will the quasi-2D state remain stable under these conditions? To answer this question, an

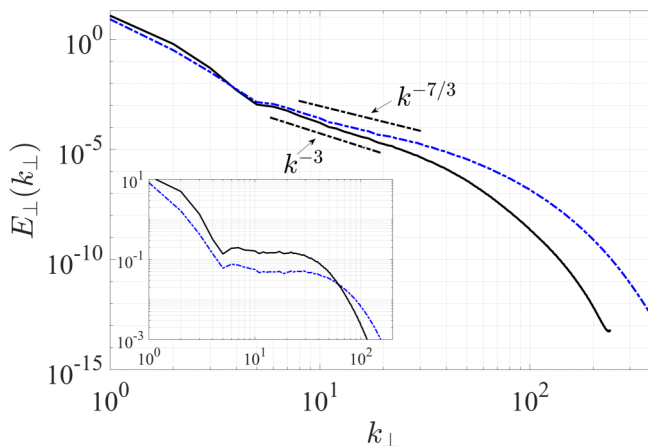


FIG. 16. Perpendicular energy spectra at $N_0 = 254$ at two values of R_0 : $R_0 = 1730$ (solid black line) and $R_0 = 5220$ (dashed-dotted blue line). The spectra compensated by k^{-3} and $k^{-7/3}$, respectively, are shown in the inset.

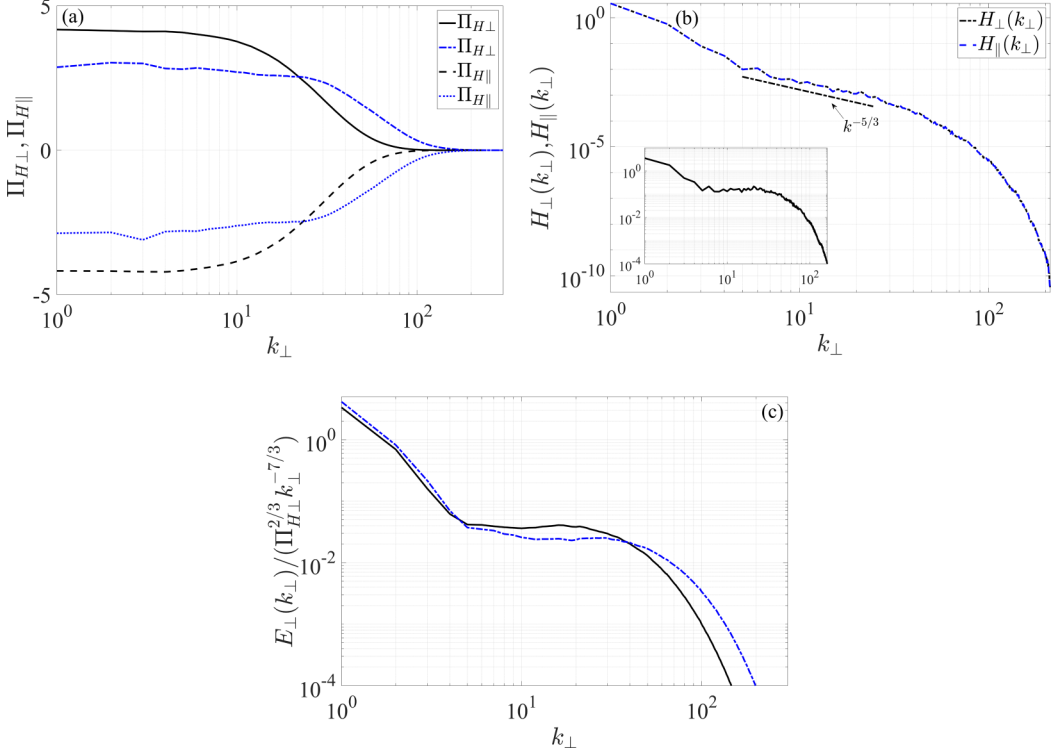


FIG. 17. (a) Perpendicular and parallel helicity fluxes, (b) helicity spectra $H_{\perp}(k_{\perp})$, $H_{\parallel}(k_{\perp})$, and (c) compensated energy spectra for $N_0 = 62$, $R_0 = 1770$ with $n = 512^3$ (solid and dashed black lines) and $N_0 = 252$, $R_0 = 5220$ with $n = 1024^3$ (dashed-dotted and dotted blue lines). Compensated spectrum $H_{\perp}(k_{\perp})/k_{\perp}^{-5/3}$ is shown in the inset in (b).

additional DNS was conducted with the same interaction parameter $N_0 = 254$ as that in the previous experiment but with a higher resolution of 1024^3 . Under these conditions, the viscosity decreased by factor of 3, leading to a corresponding increase in R_0 from 1730 to 5220. The spectrum obtained in the perpendicular plane is shown in Fig. 16 together with the spectrum at $R_0 = 1730$. With increasing R_0 , the power scaling changed from -3 to $-7/3$. The spectrum of the parallel component $E_{\parallel}(k_{\perp})$ retained its form (27) (not shown).

We now ask: What is the physics behind the $-7/3$ scaling in this experiment? The $-7/3$ spectrum is often associated with helicity cascade [71,72]. Helicity is zero in pure 2D turbulence where the vorticity vector is perpendicular to the velocity field. However, in the 2D-3C case considered here, the vorticity has a nonzero horizontal projection due to the dependence of u_3 on x_1 and x_2 , which may cause helicity flux in the normal plane. Examination of spectral amplitudes may clarify the physical mechanism governing dynamical processes leading to the $-7/3$ slope. If the flux of helicity Π_H is responsible for the observed spectrum, then it may be expected that the amplitude of the spectrum will be proportional to $\Pi_H^{2/3}$.

The fluxes of helicity in the perpendicular plane $\Pi_{H\perp}(k_{\perp})$ and along the magnetic field $\Pi_{H\parallel}(k_{\perp})$ were computed for two simulations with different settings of N_0 and R_0 , namely, $N_0 = 62$, $R_0 = 1770$ and $N_0 = 252$, $R_0 = 5220$. Both simulations gave the $-7/3$ perpendicular and -1 parallel spectra. The fluxes were computed using the following formulas:

$$\Pi_{H\perp}(k_{\perp}) = -\Re \left\langle \iiint_{V(k_{\perp})} \zeta_i^*(\mathbf{k}, t|k_{\perp}) \mathcal{F} \left(u_j \frac{\partial u_i}{\partial x_j} \right) \frac{d\mathbf{k}}{(2\pi)^3} \right\rangle, \quad i \neq 3, \quad (30)$$

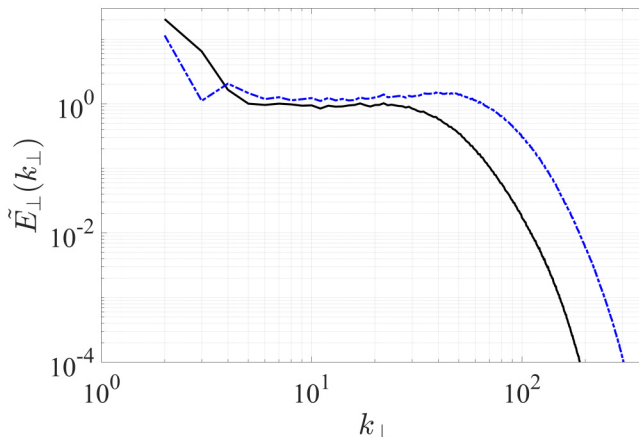


FIG. 18. Compensated energy spectrum for $N_0 = 254$, $R_0 = 1730$ with $n = 512^3$ (solid black line) and $N_0 = 806$, $R_0 = 5100$ with $n = 1024^3$ (dashed-dotted blue line).

$$\Pi_{H_{\parallel}}(k_{\perp}) = -\Re \left\langle \iiint_{V(k_{\perp})} \zeta_3^*(\mathbf{k}, t|k_{\perp}) \mathcal{F} \left(u_j \frac{\partial u_3}{\partial x_j} \right) \frac{d\mathbf{k}}{(2\pi)^3} \right\rangle. \quad (31)$$

The results presented in Fig. 17(a) indicate that the fluxes in the two simulations are significantly different, but in each simulation their values are nearly constant over a wide range of scales. Notably, the perpendicular and parallel fluxes have opposite signs but almost the same magnitudes; thus, they nearly compensate for one another in the total helicity flux. This result is not surprising, since the external forcing in our simulations does not inject helicity. Helicity spectra $H_{\perp}(k_{\perp})$, $H_{\parallel}(k_{\perp})$ are shown in Fig. 17(b). They are almost identical and seem to obey the $k^{-5/3}$ inertial range. The physical significance of this scaling is not clear. Note that our forcing does not inject helicity on average, and in a nonmagnetic case the helicity is zero. However, due to statistical nature of the forcing, some helicity input is possible at any given time. This may lead to breaking the mirror symmetry at strong fields, similarly to the report of Agoua *et al.* in their recent paper [73]. They considered statistically homogeneous, mirror-symmetric, buoyancy-driven turbulence with Joule damping, and found, we quote: “If the flow is close enough to a two-dimensional limit, spontaneous symmetry breaking leads to the generation of mean helicity” [73]. It is quite possible that we encountered a similar phenomenon. Spontaneous generation of helicity in the QS-MHD flows deserves in-depth analysis which is beyond the goals of the current research.

The energy spectra compensated by $\Pi_H^{2/3} k^{-7/3}$ are shown in Fig. 17(c). The compensated spectra are nearly constant in the range of scales between forcing and dissipation. The dimensionless constants in both simulations are close to one another, thus supporting our conjecture of a helicity cascade.

Finally, we verified that by further increasing magnetic field at constant R_0 the enstrophy cascade range with scaling (26) can be restored, replacing the helicity cascade. Figure 18 shows the compensated energy spectrum $\tilde{E}_{\perp}(k_{\perp}) = E_{\perp}(k_{\perp}) / (\eta_{\perp}^{2/3} k_{\perp}^{-3} \ln(k_{\perp}/k_{\min})^{-1/3})$ for two simulations with different settings of N_0 and R_0 : $N_0 = 254$, $R_0 = 1730$ and $N_0 = 806$, $R_0 = 5100$, respectively. Both spectra are nearly constant in the inertial range, and the dimensionless constant C_{\perp} is close to 1 in both simulations.

X. DISCUSSION AND CONCLUSIONS

Anisotropy induced by external forces and proliferation of the extra strain-related terms in the Navier-Stokes equation substantially complicate the analytical investigation of turbulent flows.

Analytical theories that predict spectral amplitudes and slopes in anisotropic flows with extra strains are, therefore, of utmost importance. It is possible to apply the QNSE theory to study turbulence anisotropization by solid-body rotation, stable stratification, or Joule friction. The theory yields important results when applied to geophysical flows, including theoretical predictions of 1D horizontal kinetic-energy spectra in the atmosphere and in oceans [74], vertical spectrum of temperature, horizontal and vertical velocity spectra in stably stratified turbulence [49,75], and transport coefficients implemented in turbulence models [76,77]. In the case of large-scale atmospheric and oceanic turbulence affected by the Earth's rotation, the theory predicts latitudinal dependence of transverse and longitudinal spectra. All the theoretical predictions agree with the observations [74].

QS-MHD is considered a useful means to study anisotropization of turbulent flows by external body forces. Laboratory experiments with electroconductive liquids in the presence of a magnetic field provide important information on this phenomenon: By changing the magnetic field induction, the process of turbulence anisotropization, and hence modification of the energy spectra and turbulent transport, can be investigated in detail in easily controlled experiments. However, laboratory MHD experiments have a serious limitation in that highly conductive fluids, like liquid metals, are needed to reach large values of the interaction parameter. Liquid metals are not transparent, which makes it virtually impossible to collect complete data on the velocity field. Thus, the only means to comprehensively investigate turbulence anisotropization under the impact of a magnetic field remain high-resolution DNS and analytical theories.

In this paper, the results of QNSE analyses of QS-MHD turbulence were compared with those obtained by DNS. Special attention was paid to spectral amplitudes and their relation to energy, enstrophy, or helicity fluxes. The theory derived for small values of the interaction parameter predicts that $-7/3$ power spectra develop in the lower band of wave numbers, while at larger k , for which the local interaction parameter $N(k) \ll 1$, the spectra revert to the Kolmogorov $-5/3$ form. The $-7/3$ range expands to higher wave numbers as the strength of the magnetic field increases. The transitional wave number k_{tr} that separates these two domains is located in the region where $N(k) \approx 1$. Both spectral laws are seen in the 1024^3 DNS with $N_0 = 1.5$, but the proximity of the $-5/3$ range to the dissipation range at this resolution makes it impossible to clearly show the transition. Much higher resolution is needed for this purpose, a resolution that allows about one decade for each of the power laws. Our simulations indicate that the intermediate range will also take close to one decade. Three decades of inertial range, undisturbed by viscous dissipation and spectral de-aliasing, is currently inaccessible to us. Thus, Kraichnan's two-parametric eddy viscosity $\nu(k|k_c)$ was employed to extend the Kolmogorov inertial range while still running on 1024^3 grid. Both spectral powers with theoretically predicted spectral amplitudes and the transitional wave number were clearly observed in the runs with TPEV.

The theoretically derived TPEV emulates the dynamic effects of small-scale (subgrid) turbulence on resolvable scales without distorting the downscale energy cascade. This allows for extension of the inertial range up to the largest resolvable wave number k_c . With our resolution of 1024^3 grid points $k_c = 483$. This is a practical implementation of Kraichnan's idea. On $1K^3$ grid points, using TPEV one can get results that otherwise need a DNS with more than $16K^3$ grid points. The TPEV was developed for isotropic turbulence, which does not hold for QS-MHD turbulence where the magnetic field induces anisotropy through the Lorentz force. However, the characteristic frequency of this action is scale independent, while the characteristic frequency of turbulent scales increases with k (for a spectrum shallower than k^{-3}). Thus, the local interaction parameter $N(k)$ decreases with k . In simulations with $N_0 = 2.2$ (which is the strongest field where we used TPEV) $N(k_c) = 0.058$. This implies that subgrid scales are only weakly affected by the field (see also Ishida and Kaneda [78]). We did not use TPEV in simulations with $N_0 > 2.2$ exactly because we want to keep SGS isotropic. We conducted a short study of "return to isotropy" on scales with small $N(k)$ and found that 1D energy spectra of all velocity components were almost identical on scales whose interaction parameter $N(k) < 0.07$. Nevertheless, the isotropic form of TPEV is an approximation whose validity and limits of applicability need to be further verified. Alternatively, correction to

TPEV in the low- $N(k_c)$ limit can be derived analytically using second-order spectral closure, but this task is beyond the goals of the current study.

The $-7/3$ power law corresponds to the lowest-order correction to the Kolmogorov spectrum [37]. The amplitude of this correction is proportional to τ_J^{-1} . Agreement remains good at values of the interaction parameter higher than those for which the theory was developed. With further increases of the magnetic field, the accuracy of the analytical spectra deteriorates, indicating that higher-order terms must be accounted for. Dimensional analysis suggests that if τ_J^{-1} remains the governing parameter, the second-order correction would be proportional to $\tau_J^{-2}k^{-3}$. The actual picture is, however, more complicated and informative. Both directional and componential anisotropization grow with increasing strength of the magnetic field. At large values of the interaction parameter, the spectra of different velocity components and/or in different directions become drastically different. Turbulent fluctuations in the direction of the magnetic field are suppressed by the field, whereas turbulent characteristics in the normal plane become independent of the field. Under these conditions, only the 2D energy spectra of the velocity components normal to \mathbf{B} and the velocity components parallel to \mathbf{B} , $E_\perp(k_\perp)$ and $E_\parallel(k_\perp)$, provide meaningful characterization of the velocity field. Simulations with large N_0 and constant R_0 show that in a strong field $E_\perp(k_\perp)$ has the form (26), which is identical to the 2D enstrophy cascade spectrum. The enstrophy cascade rate η_\perp is nearly constant in the range of wave numbers between the forcing- and dissipation ranges and does not change with increasing N_0 . Concurrently, $E_\parallel(k_\perp)$ attains the exact form of a 2D passive scalar spectrum in the inertial-convective range (27) with a constant rate of the scalar dissipation ε_\parallel . The dimensionless constants in both spectra were found to be close to those obtained in the DNS of 2D turbulence. It therefore appears that the QS-MHD turbulence becomes 2D-3C at these values of the interaction parameter. The final state is independent of \mathbf{B} , as expected of 2D turbulence in the normal plane, since the Lorentz force acting on the flow becomes potential.

With increasing R_0 at constant N_0 the enstrophy cascade becomes unstable and is replaced by helicity cascade with the $-7/3$ power energy spectrum. The enstrophy cascade is restored with an increase of N_0 . It is reasonable to assume that 2D-3C state will become unstable if R_0 is increased beyond the values pertinent to the helicity cascade, the $-5/3$ energy cascade range will develop on scales with $N(k) < 1$, with the energy flux from component u_3 being redistributed between all three component. DNS with resolution much higher than 1024^3 available to us is needed to verify this hypothesis.

The final 2D-3C state was also obtained by Favier *et al.* [26] and Reddy and Verma [28]. However, the exponential behavior of the 3D energy spectrum at large N_0 obtained by Reddy and Verma differs from the 3D spectrum obtained in our simulations. The differences could be due either to the low 256^3 resolution in their simulations or to the different type of forcing used by them [28]. Our simulations show that at large N_0 Joule dissipation acts only on the scales of energy injection (if the forcing is 3D), and angular energy transfer degenerates. Degeneration of the angular transfer at large N_0 was also reported by Reddy *et al.* [27].

Next, we examined the source of the energy supplied to the parallel velocity component. In 3D flows, pressure causes a redistribution of the energy between the components. With the collapse of velocity derivatives in the direction of the magnetic field, the flow becomes incompressible in the normal plane, and the pressure energy flux to u_3 degenerates. The direct supply of energy by an external 3D force remains the only source of ε_\parallel , as was confirmed by simulations with 3D-3C, 3D-2C, and 2D-2C forcing.

In the numerical part of this study, we consider flow in the periodic domain that represents a small volume of a homogeneous flow. We studied steady-state properties of turbulence forced on scales smaller than the box size. Thus, we might hope that the nonphysical boundary conditions (periodicity) did not unduly influence the scales smaller than the forcing scale. Although the quasi-2D turbulence in the periodic box is an idealization, it nevertheless reflects some features of real QS-MHD turbulence. At strong fields the scales larger than the forcing scale are excited and become energetic due to the inverse energy cascade, which may lead to concentration of energy on the box scale—a phenomenon known as Bose condensation [79]. Walls bounding real flows have an

important effect on structures of a size equal or larger than the distance to the wall. Sommeria and Moreau [14] have shown that at strong fields the electric currents in the Hartmann layers adjacent to transverse insulating walls act as a linear friction. Hartmann friction may prevent the energy condensation.

In our simulations the scale of the forcing was chosen in the lower end of the spectrum. Use of forcing at low wave numbers can interfere with the natural physical development of the scales larger than the forcing scales. We have not addressed these issues because our goal was to study turbulence on scales smaller than the forcing scale. Larger scales, where an inverse energy cascade develops, is a separate task that is beyond the scope of this study.

A final comment seems appropriate concerning the relevance of a QS-MHD study to other types of turbulence anisotropization. Note in this respect that the energy spectra and changes in the power exponents are often explained in terms of crossovers between 3D and 2D turbulence. In all the types of anisotropic flows mentioned above (stably stratified turbulence, turbulence in a rotating frame, and QS-MHD) -3 power spectra emerge. Theoretical analyses, supported by atmospheric and oceanic observations and laboratory experiments, reveal, however, essential differences in the physical nature of this scaling. In the case of stratification, the flow tends to develop a universal spectrum proportional to $N^2 k_z^{-3}$ for the horizontal velocity in the vertical direction, while in rotating flows affected by the Coriolis force, an $f^2 k_h^{-3}$ spectrum develops in the horizontal direction for the horizontal velocity components. (Here N and f are the frequencies of internal gravity and inertial waves, respectively.) In both cases, the -3 power spectra develop in the direction along which the phase speed of the corresponding waves is zero. There are, however, no waves in QS-MHD (the Alfvén waves degenerate into a diffusion along \mathbf{B}), and the -3 law in QS-MHD is not related to wave dynamics. There may, however, be a certain similarity between rotating and QS-MHD cases where both the Coriolis force and the Joule friction increase the velocity correlation in the parallel direction. However, contrary to QS-MHD, in geophysical flows affected by the Coriolis force, the proportionality between enstrophy flux and f^3 does not hold, and it is very likely that spectral amplitudes in the -3 power spectrum may not be closely related to the spectral enstrophy flux [74]. Comparing all three types of flow, one can see that stable stratification develops a totally different type of anisotropy. The buoyancy force causes a decrease in the correlation in the direction of the force, leading to horizontal layering and higher vertical derivatives, which means that in this case the -3 power spectrum is not related to quasi-2D dynamics.

ACKNOWLEDGMENT

This work was supported, in part, by Israel Science Foundation Grant No. 408/15.

APPENDIX

A detailed derivation of the QNSE equations has been given in previous studies [37,49,50], and only a brief summary is presented here. The governing equations are space-time Fourier transformed. They are strongly nonlinear, as the Reynolds number is large on large scales. However, on small scales, near the dissipation cutoff, viscous processes prevail, and $\text{Re} = O(1)$. The smallness of the Re facilitates the exploration of a renormalized perturbation methodology by employing “dressed” eddy viscosity and eddy diffusivity rather than their “bare” molecular values [80,81]. This methodology allows one to gradually coarse grain the flow domain by recursive elimination of small shells of small-scale modes and to calculate compensating corrections to the effective eddy viscosity and eddy diffusivity, thereby accounting for turbulent transport on the eliminated scales. Technically, this approach follows the RNG procedure of successive scale elimination [82] but differs from it in some important details. Unlike RNG, the QNSE procedure (i) does not employ fixed-point arguments, and (ii) uses a self-substitution method [48] to evaluate the product of slow and fast modes, i.e., the “cross term,” in the expansion series.

By applying the continuity equation, the pressure term may be eliminated from the space-time Fourier-transformed momentum Eq. (1) to give

$$u_\alpha(\hat{k}) = G_{\alpha\beta}(\hat{k}) \left[-\frac{i}{2} P_{\beta\gamma\sigma}(\mathbf{k}) \int u_\gamma(\hat{q}) u_\sigma(\hat{k} - \hat{q}) \frac{d\hat{q}}{(2\pi)^4} \right], \quad (\text{A1})$$

where $u_\alpha(\hat{k})$ is the Fourier-transformed velocity; $\hat{k} = (\mathbf{k}, \omega)$ is a four-dimensional vector in Fourier wave-number–frequency space, and

$$P_{\alpha\beta\gamma}(\mathbf{k}) = k_\beta P_{\alpha\gamma}(\mathbf{k}) + k_\gamma P_{\alpha\beta}(\mathbf{k}). \quad (\text{A2})$$

$P_{\alpha\beta}(\mathbf{k}) = \delta_{\alpha\beta} - k_\alpha k_\beta / k^2$ is the operator that projects any vector on the plane normal to \mathbf{k} , and $G_{\alpha\beta}(k)$ is the Green function containing all linear terms, including those caused by the external body force. At the start of the scale elimination process, the viscosity in the Green function is isotropic. It becomes anisotropic, acting differently on different velocity components and in different directions, when some of the turbulent scales are eliminated.

Equation (A1) has the form of a Langevin equation with the stochastic forcing determined by the convolution integral in (A1):

$$u_\alpha(\hat{k}) = G_{\alpha\beta}(\hat{k}) f_\beta(\hat{k}). \quad (\text{A3})$$

Mapping of the small shell of velocity modes $\Delta\Lambda$, which is subject to elimination, to the Langevin equation is an important element of the QNSE procedure. Physically, the Langevin equation represents the balance between nonlinear steering of a given mode by all other modes and damping by the renormalized viscosities. Numerous attempts to derive the stirring force $f_\beta(\hat{k})$ from first principles have so far been unsuccessful [80,83], but some of its properties follow readily from the conditions of a stochastic steady state, and flow incompressibility and homogeneity. An important requirement for the force is that $\langle f_\alpha(\mathbf{p}) f_\beta(\mathbf{q}) f_\gamma(\mathbf{k} - \mathbf{p} - \mathbf{q}) \rangle = 0$ for vector triads such that \mathbf{p} , \mathbf{q} , and $\mathbf{k} - \mathbf{p} - \mathbf{q}$ belong in the shell $\Delta\Lambda$ subject to elimination, where Λ is the effective dissipation wave number. This property alone suffices to develop a rigorous self-contained mathematical procedure for successive averaging. The force does not have to be Gaussian, although a Gaussian field would meet the above requirement. Generally, $f_\beta(\hat{k})$ may be characterized as quasinormal. The combination of the quasinormal forcing and eddy damping represented by the eddy viscosities and eddy diffusivities places the QNSE theory in the class of quasinormal eddy-damped theories of turbulence.

Scale elimination is achieved by ensemble averaging over the modes in the shell $\Delta\Lambda$, yielding a small, $O(\Delta\Lambda)$, correction to the viscosity. Along with the increase of the effective viscosity, the effective dissipation wave number, Λ , decreases. Hence, the effective Re built upon the scales pertinent to the new value of Λ is again $O(1)$, and the procedure can be repeated. At any step of the scale elimination, the correction to the inverse Green function is given by the following integral:

$$\Delta G_{\alpha\beta}^{-1}(\hat{k}) = P_{\alpha\gamma\delta}(\mathbf{k}) \int^> P_{\lambda\mu\beta}(\mathbf{k} - \mathbf{q}) U_{\gamma\mu}(\Omega, \mathbf{q}) G_{\delta\lambda}(\omega - \Omega) \frac{d\hat{q}}{(2\pi)^4}, \quad (\text{A4})$$

where $\int^> d\hat{q} = \int_{\Delta\Lambda} d^3q \int_{-\infty}^{\infty} d\Omega$. The integral contains the velocity correlation tensor $U_{\gamma\mu}(\Omega, \mathbf{q})$, which can be evaluated using the Langevin equation (A3) and the energy balance equation, which determines the forcing amplitude. Taking the limit $\Delta\Lambda \rightarrow 0$, we obtain a differential equation, relating the effective viscosity to the current value of the “moving dissipation cutoff” Λ .

The concept of viscosity implies a spectral gap between the eliminated scales, $k > \Lambda$, and resolvable (explicit) scales, $k < \Lambda$, but such a gap does not appear in the process of scale elimination. As a result, the effect of the eliminated scales on the explicit scales in the vicinity of the dissipation cutoff Λ differs from that away from it. Kraichnan [52] has shown that to obtain an adequate description of the physics, the dependence of the eddy viscosity on both the local explicit wave number k and the dissipation cutoff Λ must be taken into account. This two-parametric viscosity is denoted by $\nu(k|\Lambda)$. The QNSE theory employs an important simplification, known as the distant

interaction or spectral gap approximation, in which the limit $k/\Lambda \rightarrow 0$ is taken, and only the terms up to $O(k^2)$ are retained. Essentially, this approximation enforces a spectral gap between the resolvable and eliminated scales, and accordingly renormalized viscosities and diffusivities are taken only as functions of Λ . Although this approach introduces a certain inaccuracy, it gives reliable subgrid-scale parametrization in 3D flows featuring a direct energy cascade. The distant interaction approximation is problematic for flows with an inverse energy cascade, because the eddy viscosity $\nu(k|\Lambda)$ becomes negative at $k \rightarrow 0$ [52]. This problem arises in MHD flow, which, under the action of a strong magnetic field, becomes quasi-2D with an inverse energy cascade. Thus, the scale-elimination procedure can be used only for a weak magnetic field or on scales where the effect of Joule dissipation is weak.

In the process of scale elimination, there emerge two types of anisotropization—directional and compoential. The Green function $G_{\alpha\beta}(\hat{k})$ becomes an anisotropic tensor that contains renormalized (effective) viscosities. For the horizontal (perpendicular to \mathbf{B}) velocity components, the effective viscosities in the horizontal and the vertical (parallel to \mathbf{B}) directions are, respectively, ν_h and ν_z . For the vertical velocity component u_3 , the effective viscosities are ν_{3h} and ν_{3z} .

$$G_{\alpha\beta}(\hat{k}) = g(\hat{k})[\delta_{\alpha\beta} + A(\hat{k})P_{3\alpha}(\mathbf{k})P_{3\beta}(\mathbf{k})], \quad (\text{A5})$$

where

$$A(\hat{k}) = \frac{(v_z - \nu_{3z})k^2}{g^{-1}(\hat{k}) - (v_z - \nu_{3z})k^2 P_{33}(\mathbf{k})} \quad (\text{A6})$$

and the inverse auxiliary Green function $g^{-1}(\hat{k})$ is

$$g^{-1}(\hat{k}) = -i\omega^2 + \nu_h(k_1^2 + k_2^2) + \nu_z k_3^2 + \frac{\sigma B^2}{\rho} \frac{k_3^2}{k^2}. \quad (\text{A7})$$

It is convenient to present the scale-dependent eddy viscosities in a nondimensional form by dividing the QNSE results by the corresponding value of the eddy viscosity in the nonmagnetic case,

$$\nu_n(k) \approx 0.5\varepsilon^{1/3}k^{-2/3}, \quad (\text{A8})$$

where ε is the viscous energy dissipation rate. It has previously been shown [37] that $\nu_{3z} = \nu_{3h} \equiv \nu_3$. Other scale-dependent eddy viscosities are

$$\begin{aligned} \frac{\nu_h(k)}{\nu_n(k)} &= 1 - 0.695 \left(\frac{k_J}{k} \right)^{2/3}, \\ \frac{\nu_z(k)}{\nu_n(k)} &= 1 - 0.666 \left(\frac{k_J}{k} \right)^{2/3}, \\ \frac{\nu_3(k)}{\nu_n(k)} &= 1 - 0.106 \left(\frac{k_J}{k} \right)^{2/3}. \end{aligned} \quad (\text{A9})$$

With the eddy viscosities known (A9), the derivation of the renormalized Green function is completed and can be used for computation of velocity correlator:

$$U_{\alpha\beta}(\hat{k}) = Dk^{-3}|g(\hat{k})|^2\{P_{\alpha\beta}(\mathbf{k}) + P_{3\alpha}(\mathbf{k})P_{3\beta}(\mathbf{k})[A(\hat{k}) + A^*(\hat{k}) + |A(\hat{k})|^2P_{33}(\mathbf{k})]\} \quad (\text{A10})$$

and kinetic energy spectra. The amplitude D is computed using energy balance equation.

-
- [1] L. Blumenau, H. Branover, A. El-Boher, E. Spero, S. Sukoriansky, G. Talmage, and E. Greenspan, Liquid metal MHD energy conversion in fusion reactors, *Fusion Technol.* **10**, 914 (1986).
- [2] M. Bourgoïn, L. Marié, F. Pétréllis, C. Gasquet, A. Guigon, J. Luciani, M. Moulin, F. Namer, J. Burguete, and A. Chiffaudel, Magnetohydrodynamics measurements in the von Kármán sodium experiment, *Phys. Fluids* **14**, 3046 (2002).
- [3] A. Alemany, R. Moreau, P. L. Sulem, and U. Frisch, Influence of an external magnetic field on homogeneous MHD turbulence, *J. Mec.* **18**, 277 (1979).
- [4] P. H. Roberts, *An Introduction to Magnetohydrodynamics* (Longmans, London, 1967), Vol. 6.
- [5] L. G. Kit and A. B. Tsinober, Possibility of creating and investigating two-dimensional turbulence in a strong magnetic field (Two dimensional MHD turbulent flow generation in strong magnetic field), *Magn. Gidrodin.* **7**, 27 (1971).
- [6] Y. B. Kolesnikov and A. B. Tsinober, Experimental investigation of two-dimensional turbulence behind a grid, *Fluid Dyn.* **9**, 621 (1974).
- [7] H. Branover and P. Gershon, Experimental investigation of the origin of residual disturbances in turbulent MHD flows after laminarization, *J. Fluid Mech.* **94**, 629 (1979).
- [8] H. Branover, *Magnetohydrodynamic Flow in Ducts* (Wiley, New York, 1978).
- [9] A. D. Votsish and Y. B. Kolesnikov, Study of transition from three-dimensional to two-dimensional turbulence in a magnetic field, *Magn. Gidrodin.* **12**, 141 (1976).
- [10] S. Sukoriansky and H. Branover, Modification of turbulence structure and transfer properties in electroconductive fluids under influence of magnetic fields, in *5th Symposium on Turbulent Shear Flows* (Ithaca, NY, 1985).
- [11] S. Sukoriansky, H. Branover, and E. Greenspan, *Liquid Metal Turbulent Flow Phenomena and Their Implications on Fusion Reactor Blanket Design* (Kluwer Academic, Dordrecht, 1989), Vol. 63.
- [12] A. A. Kljukin and J. B. Kolesnikov, *MHD Turbulence Decay behind Spatial Grids* (Kluwer Academic, Dordrecht, 1989), Vol. 153.
- [13] S. Eckert, G. Gerbeth, W. Witke, and H. Langenbrunner, MHD turbulence measurements in a sodium channel flow exposed to a transverse magnetic field, *Int. J. Heat Fluid Flow* **22**, 358 (2001).
- [14] J. Sommeria and R. Moreau, Why, how, and when, MHD turbulence becomes two-dimensional, *J. Fluid Mech.* **118**, 507 (1982).
- [15] P. Caperan and A. Alemany, Turbulence homogène MHD à faible nombre de Reynolds magnétique. Etude de la transition vers la phase quasi bidimensionnelle et caractérisation de son anisotropie, *J. Mec. Theor. Appl.* **4**, 175 (1985).
- [16] S. Sukoriansky, I. Zilberman, and H. Branover, Experimental studies of turbulence in mercury flows with transverse magnetic fields, *Exp. Fluids* **4**, 11 (1986).
- [17] H. Branover, S. Sukoriansky, G. Talmage, and E. Greenspan, Turbulence and the feasibility of self-cooled liquid metal blankets for fusion reactors, *Fusion Technol.* **10**, 822 (1986).
- [18] S. Sukoriansky, D. Klaiman, H. Branover, and E. Greenspan, MHD enhancement of heat transfer and its relevance to fusion reactor blanket design, *Fusion Eng. Des.* **8**, 277 (1989).
- [19] R. H. Kraichnan, Inertial ranges in two-dimensional turbulence, *Phys. Fluids* **10**, 1417 (1967).
- [20] J. Sommeria, Experimental study of the two-dimensional inverse energy cascade in a square box, *J. Fluid Mech.* **170**, 139 (1986).
- [21] R. Klein, A. Pothérat, and A. Alferenok, Experiment on a confined electrically driven vortex pair, *Phys. Rev. E* **79**, 016304 (2009).
- [22] R. Klein and A. Pothérat, Appearance of Three Dimensionality in Wall-Bounded MHD Flows, *Phys. Rev. Lett.* **104**, 034502 (2010).
- [23] A. Pothérat and R. Klein, Why, how and when MHD turbulence at low Rm becomes three-dimensional, *J. Fluid Mech.* **761**, 168 (2014).
- [24] A. Pothérat and R. Klein, Do magnetic fields enhance turbulence at low magnetic Reynolds number? *Phys. Rev. Fluids* **2**, 063702 (2017).
- [25] O. Zikanov and A. Thess, Direct numerical simulation of forced MHD turbulence at low magnetic Reynolds number, *J. Fluid Mech.* **358**, 299 (1998).

- [26] B. F. N. Favier, F. S. Godeferd, C. Cambon, and A. Delache, On the two-dimensionalization of quasistatic magnetohydrodynamic turbulence, *Phys. Fluids* **22**, 075104 (2010).
- [27] K. S. Reddy, R. Kumar, and M. K. Verma, Anisotropic energy transfers in quasi-static magnetohydrodynamic turbulence, *Phys. Plasmas* **21**, 102310 (2014).
- [28] K. S. Reddy and M. K. Verma, Strong anisotropy in quasi-static magnetohydrodynamic turbulence for high interaction parameters, *Phys. Fluids* **26**, 025109 (2014).
- [29] P. Burattini, M. Kinet, D. Carati, and B. Knaepen, Anisotropy of velocity spectra in quasistatic magnetohydrodynamic turbulence, *Phys. Fluids* **20**, 065110 (2008).
- [30] O. Zikanov, D. Krasnov, T. Boeck, and S. Sukoriansky, Decay of turbulence in a liquid metal duct flow with transverse magnetic field, *J. Fluid Mech.* **867**, 661 (2019).
- [31] K. S. Reddy, *Anisotropic Energy Spectrum, Flux and Transfers in Quasi-Static Magnetohydrodynamic Turbulence*, PhD thesis IIT Kanpur, IIT Kanpur, 2015.
- [32] A. Poth erat and K. Kornet, The decay of wall-bounded MHD turbulence at low Rm , *J. Fluid Mech.* **783**, 605 (2015).
- [33] A. Poth erat and T. Albuoussi ere, Small scales and anisotropy in low Rm magnetohydrodynamic turbulence, *Phys. Fluids* **15**, 3170 (2003).
- [34] V. Dymkou and A. Poth erat, Spectral methods based on the least dissipative modes for wall bounded MHD flows, *Theor. Comput. Fluid Dyn.* **23**, 535 (2009).
- [35] A. Poth erat and V. Dymkou, Direct numerical simulations of low- Rm MHD turbulence based on the least dissipative modes, *J. Fluid Mech.* **655**, 174 (2010).
- [36] A. Poth erat and T. Albuoussi ere, Bounds on the attractor dimension for low- R m wall-bound magnetohydrodynamic turbulence, *Phys. Fluids* **18**, 125102 (2006).
- [37] S. Sukoriansky and E. Zemach, Theoretical study of anisotropic MHD turbulence with low magnetic Reynolds number, *Phys. Scr.* **91**, 034001 (2016).
- [38] C. Cambon, Homogeneous MHD turbulence at weak magnetic Reynolds numbers: Approach to angular-dependent spectra, in *Advances in Turbulence Studies: Progresses in Astronautics and Aeronautics*, edited by H. Branover and Y. Unger, Vol. 149, p. 131 (AIAA, Washington, DC 1991).
- [39] J. Hunt, *Rapid Distortion Theory. Lecture Notes for the ERCOFTAC Summer School* (Cambridge University Press, Cambridge, 1992).
- [40] P. Sagaut and C. Cambon, *Homogeneous Turbulence Dynamics* (Cambridge University Press, Cambridge, 2008), Vol. 10.
- [41] R. Moreau and A. Alemany, MHD flows and turbulence, in *Proceedings of Bat-Sheva International Seminar, Beer-Sheva* (Wiley, Israel, 1976) 49.
- [42] B. Knaepen and R. Moreau, Magnetohydrodynamic turbulence at low magnetic Reynolds number, *Annu Rev Fluid Mech* **40**, 25 (2008).
- [43] U. Schumann, Numerical simulation of the transition from three-to two-dimensional turbulence under a uniform magnetic field, *J. Fluid Mech.* **74**, 31 (1976).
- [44] S. A. Orszag, Lectures on the statistical theory of turbulence, in *Proceedings of the 1973 Les Houches Summer School of Theoretical Physics*, edited by R. Balian and J. L. Peube (Gordon and Breach, New York, 1973), p. 237.
- [45] C. Cambon and F. S. Godeferd, Inertial Transfers in Freely Decaying, Rotating, Stably Stratified, and Magnetohydrodynamic Turbulence, in *Progress in Turbulence Research: Progress in Astronautics and Aeronautics*, edited by H. Branover and Y. Unger, Vol. 162, p. 150 (AIAA, Washington, DC, 1994).
- [46] B. F. N. Favier, F. S. Godeferd, C. Cambon, A. Delache, and W. J. Bos, Quasi-static magnetohydrodynamic turbulence at high Reynolds number, *J. Fluid Mech.* **681**, 434 (2011).
- [47] D. Montgomery and L. Turner, Two-and-a-half-dimensional magnetohydrodynamic turbulence, *Phys. Fluids* **25**, 345 (1982).
- [48] S. Sukoriansky, B. Galperin, and I. Staroselsky, Cross-term and ϵ -expansion in RNG theory of turbulence, *Fluid Dyn. Res.* **33**, 319 (2003).
- [49] S. Sukoriansky, B. Galperin, and I. Staroselsky, A quasinormal scale elimination model of turbulent flows with stable stratification, *Phys. Fluids* **17**, 085107 (2005).

- [50] S. Sukoriansky and B. Galperin, QNSE theory of turbulence anisotropization and onset of the inverse energy cascade by solid body rotation, *J. Fluid Mech.* **805**, 384 (2016).
- [51] N. T. Baker, A. Pothérat, L. Davoust, and F. Debray, Inverse and Direct Energy Cascades in Three-Dimensional Magnetohydrodynamic Turbulence at Low Magnetic Reynolds Number, *Phys. Rev. Lett.* **120**, 224502 (2018).
- [52] R. H. Kraichnan, Eddy viscosity in two and three dimensions, *J. Atmos. Sci.* **33**, 1521 (1976).
- [53] Y. B. Kolesnikov and A. B. Tsinober, Two-dimensional turbulent flow behind a circular cylinder, *Magn. Gidrodin.* **8**, 300 (1972).
- [54] T. Gotoh, D. Fukayama, and T. Nakano, Velocity field statistics in homogeneous steady turbulence obtained using a high-resolution direct numerical simulation, *Phys. Fluids* **14**, 1065 (2002).
- [55] G. S. Patterson and S. A. Orszag, Spectral calculations of isotropic turbulence: Efficient removal of aliasing interactions, *Phys. Fluids* **14**, 2538 (1971).
- [56] W. D. McComb, *Homogeneous, Isotropic Turbulence: Phenomenology, Renormalization and Statistical Closures* (Oxford University Press, Oxford, 2014), Vol. 162.
- [57] W. P. Dannevik, V. Yakhot, and S. A. Orszag, Analytical theories of turbulence and the ε expansion, *Phys. Fluids* **30**, 2021 (1987).
- [58] A. Chekhlov, S. A. Orszag, S. Sukoriansky, B. Galperin, and I. Staroselsky, Direct numerical simulation tests of eddy viscosity in two dimensions, *Phys. Fluids* **6**, 2548 (1994).
- [59] A. Chekhlov, S. A. Orszag, S. Sukoriansky, B. Galperin, and I. Staroselsky, The effect of small-scale forcing on large-scale structures in two-dimensional flows, *Physica D* **98**, 321 (1996).
- [60] G. Falkovich, Bottleneck phenomenon in developed turbulence, *Phys. Fluids* **6**, 1411 (1994).
- [61] U. Frisch, S. Kurien, R. Pandit, W. Pauls, S. S. Ray, A. Wirth, and J. Zhu, Hyperviscosity, Galerkin Truncation, and Bottlenecks in Turbulence, *Phys. Rev. Lett.* **101**, 144501 (2008).
- [62] D. A. Donzis and K. R. Sreenivasan, The bottleneck effect and the Kolmogorov constant in isotropic turbulence, *J. Fluid Mech.* **657**, 171 (2010).
- [63] K. R. Sreenivasan, On the universality of the Kolmogorov constant, *Phys. Fluids* **7**, 2778 (1995).
- [64] N. Nakauchi, H. Oshima, and Y. Saito, Inverse energy cascade in a nearly two-dimensional turbulence, *Phys. Fluids A* **2**, 435 (1990).
- [65] G. K. Batchelor, Computation of the energy spectrum in homogeneous two-dimensional turbulence, *Phys. Fluids* **12**, II-233 (1969).
- [66] R. H. Kraichnan, Inertial-range transfer in two- and three-dimensional turbulence, *J. Fluid Mech.* **47**, 525 (1971).
- [67] Y. Kaneda, Inertial range of two-dimensional turbulence in a Lagrangian renormalized approximation, *Phys. Fluids* **30**, 2672 (1987).
- [68] T. Gotoh, Energy spectrum in the inertial and dissipation ranges of two-dimensional steady turbulence, *Phys. Rev. E* **57**, 2984 (1998).
- [69] M. Lesieur and J. Herring, Diffusion of a passive scalar in two-dimensional turbulence, *J. Fluid Mech.* **161**, 77 (1985).
- [70] T. Gotoh, Passive scalar diffusion in two dimensional turbulence in the Lagrangian renormalized approximation, *J. Phys. Soc. Jpn.* **58**, 2365 (1989).
- [71] H. Branover, A. Eidelman, M. Nagorny, and M. Kireev, Magnetohydrodynamic Simulation of Quasi-Two-Dimensional Geophysical Turbulence, in *Progress in Turbulence Research: Progress in Astronautics and Aeronautics*, edited by H. Branover and Y. Unger, Vol. 162 (AIAA, Washington, DC, 1994), p. 64.
- [72] E. Golbraikh, O. G. Chkhetiani, and S. S. Moiseev, The role of helicity in turbulent MHD flows, *J. Exp. Theor. Phys.* **87**, 95 (1998).
- [73] W. Agoua, B. Favier, A. Delache, A. Briard, and W. J. Bos, Spontaneous generation and reversal of helicity in anisotropic turbulence, *Phys. Rev. E* **103**, L061101 (2021).
- [74] B. Galperin and S. Sukoriansky, Quasinormal scale elimination theory of the anisotropic energy spectra of atmospheric and oceanic turbulence, *Phys. Rev. Fluids* **5**, 063803 (2020).
- [75] S. Sukoriansky and B. Galperin, An analytical theory of the buoyancy–Kolmogorov subrange transition in turbulent flows with stable stratification, *Philos. Trans. R. Soc., A* **371**, 20120212 (2013).

- [76] S. Sukoriansky, B. Galperin, and V. Perov, Application of a new spectral theory of stably stratified turbulence to the atmospheric boundary layer over sea ice, [Boundary Layer Meteorol.](#) **117**, 231 (2005).
- [77] S. Sukoriansky, N. Dikovskaya, and B. Galperin, Transport of momentum and scalar in turbulent flows with anisotropic dispersive waves, [Geophys. Res. Lett.](#) **36**, L14609 (2009).
- [78] T. Ishida and Y. Kaneda, Small-scale anisotropy in magnetohydrodynamic turbulence under a strong uniform magnetic field, [Phys. Fluids](#) **19**, 075104 (2007).
- [79] L. M. Smith and V. Yakhot, Bose Condensation and Small-Scale Structure Generation in a Random Force Driven 2D Turbulence, [Phys. Rev. Lett.](#) **71**, 352 (1993).
- [80] W. D. McComb, *The Physics of Fluid Turbulence* (Oxford University Press, Oxford, 1990).
- [81] W. D. McComb, Theory of turbulence, [Rep. Prog. Phys.](#) **58**, 1117 (1995).
- [82] V. Yakhot and S. A. Orszag, Renormalization group analysis of turbulence. I. Basic theory, [J. Sci. Comput.](#) **1**, 3 (1986).
- [83] V. M. Canuto and M. S. Dubovikov, A dynamical model for turbulence. I. General formalism, [Phys. Fluids](#) **8**, 571 (1996).